HHS Public Access

Author manuscript

Biomaterials. Author manuscript; available in PMC 2020 December 01.

Published in final edited form as:

Biomaterials. 2019 December ; 224: 119467. doi:10.1016/j.biomaterials.2019.119467.

Manganese Dioxide Nanoparticles Protect Cartilage from Inflammation-Induced Oxidative Stress

Shreedevi Kumar[1], **Isaac M. Adjei, PhD**[1], **Shannon Brown, PhD**[1], **Olivia Liseth**[1], **Blanka Sharma, PhD**[1,*]

[1]J. Crayton Pruitt Family Department of Biomedical Engineering, University of Florida, 1275 Center Drive Biomedical Sciences Building JG-56, P.O. Box 116131, Gainesville, FL 32611-6131

Abstract

Oxidative stress has been implicated in the pathogenesis of osteoarthritis and has become an important therapeutic target. Investigations of various antioxidant supplements, reactive oxidative species (ROS) pathway mediators, and free radical scavengers for treating osteoarthritis have demonstrated common disadvantages including poor bioavailability and stability, as well as rapid joint clearance or release profiles from delivery vehicles. Moreover, these therapies do not target cartilage, which irreversibly degenerates in the presence of oxidative stress. The goal of this study was to engineer a nanoparticle system capable of sustained retention in the joint space, localization to cartilage, and mitigation of oxidative stress. Towards this goal, ROS scavenging manganese dioxide nanoparticles with physicochemical properties (less than 20 nm and cationic) that facilitate their uptake into cartilage were developed and characterized. These particles penetrated through the depth of cartilage explants and were found both in the extracellular matrix as well as intracellularly within the resident chondrocytes. Furthermore, the particles demonstrated chondroprotection of cytokine-challenged cartilage explants by reducing the loss of glycosaminoglycans and release of nitric oxide. Quantitative PCR analysis revealed that the particles mitigated impacts of oxidative stress related genes in cytokine-challenged chondrocytes. When injected intra-articularly into rats, the particles persisted in the joint space over one week, with 75% of the initial signal remaining in the joint. Biodistribution and histological analysis revealed accumulation of particles at the chondral surfaces and colocalization of the particles with the lacunae of chondrocytes. The results suggest that the manganese dioxide nanoparticles could be a promising approach for the chondroprotection of osteoarthritic cartilage.

Graphical Abstract

[*]Corresponding author: J. Crayton Pruitt Family Department of Biomedical Engineering, University of Florida, 1275 Center Drive Biomedical Sciences Building JG-56, P.O. Box 116131, Gainesville, FL 32611-6131, blanka.sharma@bme.ufl.edu, Phone: (352) 273 - 9329, Fax: (352) 273 - 9221.

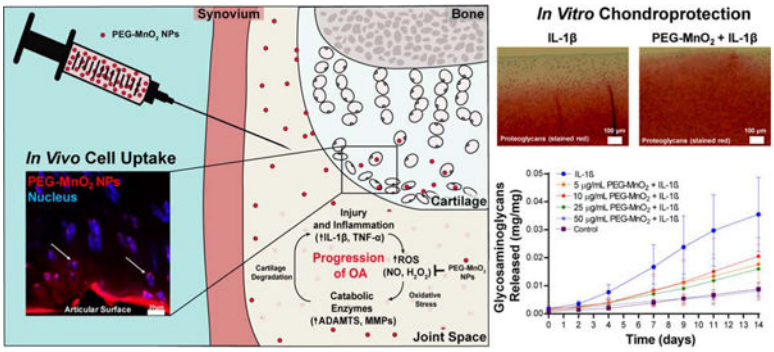

Keywords

Osteoarthritis; Oxidative Stress; Cartilage; Nanoparticle; Drug Delivery

Osteoarthritis (OA) is a degenerative joint disease that impacts over 30 million Americans [1] and is the leading cause of activity limitation and absenteeism among working adults in the United States [1]. The prevalence of OA is expected to increase, with estimates that by 2030, approximately 25% of the adult population is expected to suffer from OA [2]. There is currently no cure or disease-modifying treatment available for this disease and patients are commonly prescribed palliative therapies such as non-steroidal anti-inflammatory drugs (NSAIDS) and analgesics. Oxidative stress has been implicated in the onset and progression of OA, and studies suggest the use of antioxidants or agents that target reactive oxygen species (ROS) mechanisms in the joint could reduce OA severity without the adverse effects of chronic use of pain medication [3,4].

The pathogenesis of OA is marked by cartilage erosion, abnormal bone remodeling, and chronic low-grade inflammation of the synovium. The production of pro-inflammatory cytokines such as interleukin-1 (IL-1) within the joint leads to the generation of ROS such as peroxides, hydroxylated radicals, and nitric oxide (NO) and concomitant downregulation of antioxidants such as superoxide dismutase (SOD), catalase (CAT), and glutathione peroxidase (GPX) [5,6]. The resulting oxidative stress leads to upregulation of catabolic enzymes, extracellular matrix (ECM) degradation, decreased matrix synthesis, joint inflammation, and chondrocyte death and senescence, thereby contributing to the overall progression of the disease [5].

Given the complex etiology of OA, several risk factors for the incidence and progression of the disease have been identified. Furthermore, a delineation of the different clinical phenotypes of the disease, including metabolic, ageing-related, post-traumatic, genetic, and pain-related OA, is generally accepted [7]. The presence of oxidative stress is common across the spectrum of OA phenotypes. Aging is a key risk factor for OA and several mechanisms are upregulated with aging that could threaten the homeostatic balance between ROS and antioxidants in the joint [8]. For instance, with mitochondria being a key source of ROS in the cell, chondrocyte mitochondrial dysfunction that occurs with aging has been shown to cause imbalances in ROS production and antioxidant capacities of the cells [9]. Cellular senescence and apoptosis are also prevalent in aged cartilage and are characterized

by accumulation of cellular damage, which in turn upregulates ROS in the joint [10]. In post-traumatic osteoarthritis (PTOA), release of ROS occurs from mitochondria within chondrocytes upon excessive mechanical loading on the articular cartilage leading to cartilage cell death, inflammation of joint tissues and degradation of matrix components [11]. Clearly, oxidative stress is implicated in the progression of various phenotypes of OA, making it a therapeutic target that could impact a broad spectrum of patients.

Currently, therapies such as antioxidant supplements, mediators of various ROS pathways, and free radical scavengers are being investigated to target the oxidative stress present in OA pathogenesis. Antioxidant supplements have had variable success when used to treat OA and are often plagued by poor stability and bioavailability. Indeed, clinical testing of antioxidant vitamins such as Vitamin A, C, E or selenium have either shown contradictory findings or been ineffective in treating arthritis [12,13]. Curcumin, for example, has been shown to inhibit matrix degradation and decrease production of matrix metalloproteinases (MMPs) *in vitro* [3]. However, curcumin's poor water solubility, short biological half-life, and low bioavailability after oral administration has hampered its adoption in clinical use [14]. To overcome bioavailability and stability issues, direct intra-injection of antioxidants such as Vitamin C [15] and polyphenols like resveratrol [16–18] or combination treatments of epigallocatechin gallate and tannic acid [19] have been explored. However, even with intra-articular injections, small molecules are rapidly cleared from the joint within hours *via* synovial vasculature and larger macromolecules within days *via* synovial lymphatics [20–22]. As a result, high doses and/or frequent injections are required to observe therapeutic benefits [23]. While controlled release systems have been explored for a number of OA drugs with limited success [24,25], their application to oxidative stress mechanisms is sparse, and challenges obtaining effective drug loading and release profiles persist [26].

Often overlooked are the additional requirements for tissue targeting – while oxidative stress is experienced throughout the joint, each tissue poses unique barriers to localization and uptake of therapeutics [27]. Cartilage is particularly vulnerable to the effects of oxidative stress and also a difficult target for drug delivery. Cartilage is avascular, aneural, and comprises a sparse population of chondrocytes within a dense ECM. As such, there are limited mechanisms for replenishing dead chondrocytes. Buildup of superoxide anions (O_2^-) and NO in cartilage leads to ROS-induced DNA damage and apoptosis, irreversible cartilage degeneration, and propagation of cyclic joint inflammation [5,28,29]. Therefore, the need to get therapeutically relevant dosages of antioxidants into the cartilage tissue itself is critical for chondroprotection against the deleterious effects of oxidative stress.

The overall goal of this study was to target OA-related oxidative stress mechanisms while overcoming issues of poor drug bioavailability and cartilage localization. Specifically, we developed ROS-scavenging nanoparticles (NPs) made from manganese dioxide (MnO_2) with physicochemical properties that facilitate their cartilage penetration and prolonged retention in the joint. Manganese dioxide catalyzes the breakdown of hydrogen peroxide (H_2O_2) [30], a key radical that is derived from O_2^-, one of the main reactive oxidative species produced by chondrocytes [31,32]. These properties of MnO_2 particles are being explored for scavenging ROS in other inflammatory conditions such as arthrosclerosis and diabetes. For example, microparticles comprised of a MnO_2 core demonstrated continuous scavenging of

H_2O_2 in cultures mimetic of inflamed vasculature [33]. Manganese dioxide particles have also exhibited free radical scavenging and cytoprotection of pancreatic islets of Langerhans *in vitro* [34]. Systemic biocompatibility of MnO_2 NPs have been demonstrated *in vivo* in tumor models, where MnO_2 is being utilized as an MRI contrast agent [35,36]. Importantly, the use of a bioactive NP that is made of the scavenging material, MnO_2, could address issues of rapid release profiles of drug-loaded nanocarriers.

In this study, it was hypothesized that MnO_2 NPs will protect cartilage from inflammation-induced oxidative stress. To test this hypothesis, MnO_2 NPs were first engineered to have physicochemical properties that facilitate uptake and penetration through cartilage followed by evaluation of their chondroprotective capacity. This study represents the first application of MnO_2 NPs to cartilage protection and osteoarthritis.

Results

Formulation and Characterization of NPs.

Given that cartilage comprises a dense collagen type II fibrillar network with a mesh size of ~50 – 60 nm [37,38] and anionic proteoglycans with ~20 nm spacing [39] between side chains, we set out to engineer particles that were less than 20 nm and cationic to facilitate cartilage retention [40–46]. Plain MnO_2 NPs were successfully synthesized *via* a redox reaction between potassium permanganate ($KMnO_4$) and poly(allyl amine) hydrochloride (PAH) as previously reported [36,47,48]. The reaction was confirmed by absorbance spectrum, which shows the disappearance of $KMnO_4$ peaks and emergence of a 300 nm peak characteristic of colloidal MnO_2. (Fig. 1A). The resulting NPs had a hydrodynamic diameter (number-weighted) of 12.85 nm (polydispersity = 0.239) (Fig. 1D) and a zeta potential of +52.12 mV (Fig. 1E). However, these plain MnO_2 NPs were not colloidally stable in saline or biological fluids such as synovial fluid (Fig. 1B). Conjugation of polyethylene glycol (PEG) to the MnO_2 NPs (PEG-MnO_2) conferred colloidal stability in both saline and synovial fluid (Fig. 1B) while maintaining a particle size less than 20 nm and a positive zeta potential (Fig. 1D and E). Specifically, PEGylation of MnO_2 NPs maintained a hydrodynamic diameter (number weighted) of 10.92 nm (polydispersity = 0.194) (Fig. 1D) and decreased the zeta potential of the particles to +29.11 mV (Fig. 1E). The size of the PEG-MnO_2 NPs was confirmed by transmission electron microscopy (TEM) to be 15 nm (±4.3nm) (Fig. 1C). These properties did not change significantly when the NPs were labeled with a fluorescent dye, such as Alexa Fluor 750 (Fig. 1D and E).

The conjugation of PEG to MnO_2 was confirmed using Fourier-transform infrared spectroscopy (FTIR) by the presence of carbon-hydrogen bonds and carbon-oxygen single bonds which are characteristic of PEG (Fig. 1F). To further characterize the presence of PEG and quantify the proportion of organic and inorganic components in the PEG-MnO_2 NPs, thermogravimetric analysis (TGA) was performed on both plain MnO_2 and PEG-MnO_2 NPs in the temperature range of 10 – 600°C (Fig. 1G). The resulting TGA thermogram indicated the plain MnO_2 NPs comprise approximately 58% inorganic MnO_2 by weight while PEG-MnO_2 comprise approximately 35% inorganic MnO_2. Assuming the mass of PAH and any trace moisture on the plain MnO_2 and the PEG-MnO_2 are similar, the difference of 23% in the masses following combustion at 600°C could be attributed to PEG on the PEG-MnO_2.

The PEG-MnO_2 NPs effectively scavenged H_2O_2, with 5 μg/mL PEG-MnO_2 NPs neutralizing 65% of 100 μM H_2O_2 (Fig. 1H) after an hour of incubation, suggesting that the NPs demonstrated scavenging capacity as intended. Alexa Fluor 594 labeled PEG-MnO_2 NPs also scavenged for H_2O_2 with 5 μg/mL of NPs neutralizing 17% of 100 μM H_2O_2 (Fig. S1) after an hour of incubation. Given this reduction in scavenging ability, labeled particles were only used for cell uptake and biodistribution studies where NPs needed to be tracked; all biological and functional assays were conducted with unlabeled PEG-MnO_2 NPs. As expected, O_2 was generated concurrent to scavenging of H_2O_2 by the NPs. Quantification indicated a 3-fold increase in O_2 generated as the concentration of PEG-MnO_2 NPs incubated in 100 μM H_2O_2 was increased from 2.5 μg/mL to 5 μg/mL and a 6.9-fold increase when the concentration was increased from 2.5 μg/mL to 10 μg/mL (Fig. 1I).

Cell Uptake and Cytocompatibility of PEG-MnO_2 NPs.

Particle uptake and cytocompatibility was assessed in chondrocytes as well as other cells within the joint that could be readily exposed to the PEG-MnO_2 NPs upon intra-articular injection. Chondrocytes, the primary target of the PEG-MnO_2 NPs, internalized the NPs with modest endosomal escape. A Mander's overlap coefficient analysis for co-localization of NPs with endolysosomes indicated that 19% of NPs escaped from endosomes at 24-hours after incubation (Fig. 2A). The PEG-MnO_2 NPs were cytocompatible with chondrocytes in monolayer, as determined by the MTS assay for metabolic activity, up to a concentration of 100 μg/mL (Fig. 2B). Similarly, the PEG-MnO_2 NPs did not impact metabolic activity of synoviocytes, mesenchymal stem cells, RAW 264.7 macrophages or primary rat bone-marrow derived macrophages (BMDMs) at concentrations up to 100 μg/mL (Fig. 2C). In addition to the MTS assay, an LDH assay was performed to further characterize any possible cytotoxicity. The PEG-MnO_2 NPs did not significantly increase the leakage of lactate dehydrogenase (LDH) by the cells at concentrations up to 100 μg/mL (Fig. 2D) compared to untreated controls. In further biological and functional assays, PEG-MnO_2 NPs concentrations between 5 – 100 μg/mL were used.

Though cytocompatibility was observed across different species of macrophages, further experimentation was conducted to assess any adverse effects to macrophage activation. Interestingly, the PEG-MnO_2 NPs actually downregulated the secretion of pro-inflammatory cytokine TNF-α (Fig. S2) by classically activated rat BMDMs in a dose-dependent manner. At 5 μg/mL of PEG-MnO_2 NPs, TNF-α secretion was decreased by 3.8-fold while at 100 μg/mL of the NPs TNF-α secretion decreased by 9.0-fold.

Uptake and Cytocompatibility of PEG-MnO_2 NPs in *Ex-Vivo* Cartilage Explants.

The interaction and distribution of PEG-MnO_2 NPs in three-dimensional cartilage explants was evaluated, to more closely mimic the manner in which the particles would interact with cartilage *in vivo*. Cartilage explants were harvested from bovine femoropatellar joints, which have cartilage thicknesses comparable to human cartilage. Studies in which fluorescently tagged PEG-MnO_2 NPs were incubated with cartilage explants for 24-hours revealed high signal of particles in the first 30 μm of biopsy depth (Fig. 3A) with particle penetration throughout the whole thickness of the biopsy (Fig. S3). Of note, NPs were found in the matrix as well as localized near cell nuclei, suggesting endocytosis by resident chondrocytes

(white arrows in Fig. 3A and Fig. S3). Following 24-hour exposure to PEG-MnO_2 NPs in chondrocyte media, the cartilage explants remained viable, as evidenced by LIVE/DEAD (Fig. 3B) and TUNEL assays (Fig. 3C, positive control shown in Fig. S4). During this time, the explants did not exhibit changes to extracellular matrix as indicated by Safranin-O staining (Fig. 3D). These results suggest the particle properties facilitate penetration and uptake into cartilage and confirm cytocompatibility as observed in cell monolayer studies.

Chondroprotection of PEG-MnO_2 NPs.

The chondroprotective characteristics of the PEG-MnO_2 NPs were tested in a cytokine-challenged cartilage explant model, whereby cartilage explants were incubated with IL-1β to induce oxidative stress and inflammation-mediated cartilage degeneration [49]. IL-1β is a major catabolic cytokine in the initiation and progression of OA, and is involved in the stimulation of catabolic enzymes such as MMPs, which degrade the ECM of cartilage, leading to the release of GAGs [50]. IL-1β also stimulates inducible nitric oxide synthase (iNOS) [51], a destructive mediator that inhibits collagen and proteoglycan synthesis, and induces chondrocyte cell death. To mimic these OA conditions *in vitro*, bovine cartilage explants were challenged by 10 ng/mL IL-1β over 2 weeks, with experimental groups receiving one dose of PEG-MnO_2 NPs each week.

Preliminary dose-response studies revealed that concentrations of 5, 10, 25 and 50 μg/mL PEG-MnO_2 NPs led to significant decreases in GAG and NO released by cartilage challenged by IL-1β relative to the untreated control (Fig. S5). While the 50 μg/mL dosage was most effective at reducing GAG and NO release, doses of 5 – 25 μg/mL had statistically similar outcomes. The minimum effective dose tested of 5 μg/mL was selected for further *in vitro* studies.

The viability of explants was determined using both a LIVE/DEAD staining kit (Fig. 4A) and TUNEL assay (Fig. 4B, positive control shown in Fig. S4). While the LIVE/DEAD staining did not indicate statistically significant differences in viability across groups (Fig. 4D), the TUNEL assay revealed a 1.7-fold reduction in apoptosis in cytokine challenged explants treated with PEG-MnO_2 NPs (Fig. 4E) compared to cytokine challenged controls. Treatment with PEG-MnO_2 NPs also preserved the ECM of cytokine-challenged explants over the 2-week study, as evidenced in Safranin-O staining (Fig. 4C). Explants treated with IL-1β alone exhibited decreased staining due to loss of proteoglycan components from the articular surface. When treated by PEG-MnO_2, the cytokine-challenged explants showed consistent staining of the proteoglycans throughout most of the ECM by Safranin-O, with mild loss of proteoglycans near the surface when compared to the control explants. Histological observations were confirmed by quantification of GAG release into the media, where cytokine-challenged explants treated with PEG-MnO_2 experienced a 30% decrease in GAG loss compared to cytokine-challenged controls (Fig. 4C). PEG-MnO_2 NPs also significantly decreased NO production by the cytokine-challenged cartilage explants by 40% compared to cytokine-challenged controls (Fig. 4E). Importantly, the treatment of cartilage explants with PEG-MnO_2 NPs in the absence of cytokines did not cause any adverse effects, as GAG and NO release were similar to untreated controls.

Impact of PEG-MnO_2 NPs on Gene Expression of Cytokine-Challenged Chondrocytes.

To understand the mechanisms involved in PEG-MnO_2 NP-mediated chondroprotection, quantitative gene expression was analyzed in chondrocytes challenged with 10 ng/mL IL-1β in the presence and absence of 5 μg/mL PEG-MnO_2 NPs. Serum-starved chondrocytes were exposed to (1) control conditions (2) 10 ng/mL IL-1β (3) 5 μg/mL PEG-MnO_2 or (4) 10 ng/mL IL-1β and 5 μg/mL PEG-MnO_2 simultaneously in Earle's Balanced Salt Solution (EBSS) for 24-hours. The treatments were removed and fresh chondrocyte media was added to them, with the cytokine-challenged chondrocytes receiving continued exposure to 10 ng/mL IL-1β. RNA was extracted after 48-hours of incubation in chondrocyte media.

Overall, PEG-MnO_2 NPs prevented the upregulation of OA-related catabolic mediators in cytokine challenged chondrocytes. As previously mentioned, iNOS causes the upregulation of NO, a major pro-inflammatory and destructive mediator in OA [51]. While the expression of iNOS was upregulated by 1.9-fold from control conditions (Fig. 5A) in cytokine-challenged chondrocytes, treatment with PEG-MnO_2 NPs in the presence of IL-1β maintained iNOS expression in chondrocytes at levels similar to healthy control chondrocytes (*i.e.* no cytokine challenge). Catabolic enzymes MMP1 and MMP13, both of which are involved in cartilage ECM degradation, were also examined. MMP13 in particular is considered a major catabolic effector in OA due to its ability to cleave type 2 collagen in articular cartilage [52], leading to GAG loss as well as collagen degradation. The expressions of both MMP1 and MMP13 (Fig 5B and C) were significantly upregulated by 125.8-fold and 70.5-fold, respectively, from control conditions when the chondrocytes were cytokine-challenged. The expression of both genes was maintained at baseline levels when the cytokine-challenged cells were treated with PEG-MnO_2 NPs. The expression of a disintegrin and metalloproteinase with thrombospondin motifs 5 (ADAMTS5) (Fig. 5D), which plays a key role in proteoglycan degradation, was upregulated by 3.5-fold in cells challenged by 10 ng/mL IL-1β but remained at control levels when also treated by PEG-MnO_2 NPs. In contrast, ADAMTS4 (Fig. 5E) expression was not upregulated from baseline conditions in cytokine-challenged cells. This is in line with studies in murine arthritis models suggesting that ADAMTS5 may play a more dominant role in OA pathogenesis than ADAMTS4 [53,54].

PEG-MnO_2 NPs also impacted the expression of antioxidant genes by cytokine-challenged chondrocytes. Challenge with IL-1β stimulated the expression of antioxidants (Fig. 6), which may occur to counter initial redox imbalances [55–57], including the upregulation of GPX by 10.2-fold, manganese superoxide dismutase (MnSOD) by 43.4-fold, and extracellular superoxide dismutase (ECSOD) by 1.3-fold in chondrocytes. While treatment with PEG-MnO_2 NPs resulted in maintenance of GPX gene expression at baseline levels and significantly lowered levels of MnSOD expression, the NPs led to ECSOD gene expression being downregulated below baseline in cytokine-challenged cells. Surprisingly, the expression of CAT, which primarily functions to decompose H_2O_2 to water and oxygen, was downregulated in all groups relative to control chondrocytes. Treatment of cytokine-challenged chondrocytes with PEG-MnO_2 NPs reduced or eliminated the need for antioxidant upregulation.

The gene expression levels of antioxidant regulators involved were further evaluated. Consistent with antioxidant gene expression, many antioxidant regulators were upregulated when chondrocytes were challenged by IL-1β but remained at baseline when treated by PEG-MnO_2 NPs. These included nuclear factor erythroid 2-like 2 (NRF2), which is the master regulator of antioxidative responses and controls the expression of many downstream antioxidant mediators including Heme Oxygenase 1 (HMOX1) and NAD(P)H quinone dehydrogenase 1 (NQO1). NRF2 is regulated by the repressor protein Kelch-like ECH-associated protein 1 (KEAP1) [58]. The modulation of NRF2 is heavily implicated in the aggravation of joint diseases such as rheumatoid arthritis (RA) and OA [59]. While IL-1β upregulated the gene expression of NRF2 (Fig. 7A), KEAP1 (Fig. 7B) and HMOX1 (Fig. 7C) by approximately 2-fold, treatment with PEG-MnO_2 NPs maintained the expression of these genes at control levels and downregulated expression of NQO1 (Fig. 7D) below control levels. In this manner, the NRF2-KEAP1-ARE (antioxidant responsive element) antioxidant pathway is likely impacted by the presence of the ROS scavenging PEG-MnO_2 NPs. Thioredoxin 1 (TXN1), a key mediator in the thioredoxin superfamily of proteins that participate in many redox reactions in cells, is upregulated in human RA and OA tissues, though mRNA and protein expression of TXN1 in RA tissues was higher than that in OA tissues [60]. The gene expression for this enzyme was upregulated by 2.4-fold in chondrocytes incubated with IL-1β but remained at baseline levels when also treated with PEG-MnO_2 NPs (Fig. 7E). A related enzyme, peroxiredoxin 1 (PRDX1), has demonstrated protection of rat articular chondrocytes from IL-1β-induced apoptosis when overexpressed, implying the likely upregulation of PRDX1 gene expression by the cells' endogenous antioxidant system when chondrocytes are exposed to inflammatory conditions [61]. Once again, gene expression of PRDX1 was stimulated slightly by 1.5-fold when chondrocytes were incubated with IL-1β but was maintained at control levels when the cytokine-challenged chondrocytes were treated by PEG-MnO_2 NPs (Fig. 7F). The expression of several other antioxidant genes that are commonly associated with oxidative stress in metabolic pathways, though not heavily implicated in OA pathogenesis, were examined. Sterol regulatory element-binding protein 1 (SREBP1) (Fig. 7G), peroxisome proliferator-activated receptor α (PPARα) (Fig. 7H) and carnitine palmitoyltransferase 2 (CPT2) (Fig. 7I) were upregulated by approximately 2-fold when chondrocytes were cytokine-challenged. However, treatment with PEG-MnO_2 NPs maintained the expression of these genes at control levels and even downregulated expression of acetyl-CoA carboxylase 1 (ACACA1) (Fig. 7J) below control levels. Overall, the PEG-MnO_2 NPs consistently mitigated the upregulation of antioxidant mediators by IL-1β such that their gene expression profiles are similar to healthy chondrocytes that have not been exposed to an inflammatory insult.

The gene expression of matrix building components such as collagen 2 (COL2) and aggrecan (ACAN) were both upregulated by 2 to 3-fold in the presence of IL-1β, which is in line with studies showing an increase in anabolic factors during early responses to cartilage degeneration [62]. In contrast, cytokine challenged chondrocytes treated with the PEG-MnO_2 NPs expressed COL2 and ACAN at similar levels to healthy control chondrocytes.

Retention and Biodistribution of PEG-MnO_2 NPs *in vivo.*

To ultimately move this promising chondroprotective strategy *in vivo*, the retention and cartilage localization of the particles within the joint were characterized. *In vivo* studies demonstrated favorable joint retention and cartilage localization of Alexa Fluor 750 labeled PEG-MnO_2 NPs after intra-articular injection in rats. The PEG-MnO_2 NPs were retained in the joint space for at least 7 days after *in vivo* intra-articular injection, with 75% of the initial signal remaining in joints at the end of the study. (Fig. 9).

Indeed, *ex vivo* imaging of joint tissues revealed accumulation of particles at the chondral surfaces (patella, femoral condyles, and tibial plateau) after 7 days (Fig. 10A) with minimal accumulation in extra-articular organs, including heart, lungs, spleen, liver and kidneys (Fig. 10B). In a separate cohort of animals, the distribution of Alexa Fluor 594 labeled PEG-MnO_2 NPs in whole joint histology sections was evaluated 2 days post-injection. Analysis of the whole-joint histology confirmed penetration of PEG-MnO_2 NPs into cartilage *in vivo* (Fig. 10C). A gradient of NPs was observed in cartilage with the greatest levels at the articular surface which progressively decreased with depth into the cartilage. Furthermore, the NPs were found colocalized with chondrocytes in lacunae (indicated by white arrows in Fig. 10C), suggesting uptake of the NPs by the chondrocytes and thereby corroborating *in vitro* findings.

Long-Term Cytocompatibility of PEG-MnO_2 NPs *in vivo.*

To evaluate long-term compatibility of the PEG-MnO_2 NPs in the joint, histological analysis was conducted 6 weeks post injection. Quantitative measures in the 2010 OARSI (Osteoarthritis Research Society International) recommendations for the rat [63] were used in combination with a histological grading software, GEKO [64], to assess joint health. This analysis revealed no long-term adverse effects of intra-articular PEG-MnO_2 NP injection into healthy animals. Histological parameters such as synovium thickness (Fig. 11), total cartilage degeneration width, and cartilage matrix loss width were comparable in knees injected with the NPs and those injected with saline after 6 weeks, confirming the biocompatibility of the particles *in vivo* (Table S1).

Discussion

The current work highlights a promising free radical scavenging nanotherapeutic strategy, PEGylated MnO_2 NPs, customized for delivery to osteoarthritic cartilage. Free radical scavengers have been investigated in the past for the treatment of OA with varying outcomes and limitations. Exogenous SOD or catalase conjugated to polymers like PEG or pyran (divinylether maleic acid) have been tested in clinical trials for various diseases including arthritis, pulmonary disease and ischemic tissue damage [20,21]. Orgotein, the drug version of Cu-Zn SOD, improved clinical outcomes in OA patients compared to the corticosteroid control group over a 6 month period, but only when injected at a high dose and frequency [23]. More recently, Tempol, a superoxide dismutase mimic [65], and N-[2-bromo-4-(phenylsulfonyl)-3-thienyl]-2-chlorobenzamide (BNTA), a small molecule that induces the expression of SOD3, [66] have been explored as free radical scavenging strategies in preclinical OA models, but have so far required administration prior to injury induction or

frequent (*e.g.* twice weekly) intra-articular injections. These studies highlight the persistent challenge with intra-articular therapies of rapid clearance of drugs from the joint space, which undermines therapeutic efficacy and/or clinical translation. Biomaterials have been applied as drug carriers to prolong the retention of drugs in the joint and reduce the frequency of administration [22], however few have been examined for the delivery of antioxidants and/or ROS scavengers. In some cases, disease-associated ROS is used as a trigger for environmentally-responsive drug delivery of OA therapeutics [67] and other cargo molecules [68–71], but the ROS is not the target itself. Here, PEG-MnO_2 NPs were leveraged for their inherent ROS scavenging properties. This strategy has similarly been explored using gold NPs [72,73] in a models of RA *via* intra-articular injection and cerium oxide NPs in an *in vitro* cartilage model of OA [74], however a key advantage of MnO_2 is that it is degradable in acidic, yet physiologic, conditions to water-soluble Mn^{2+} ions [75,76] and can be readily cleared from the body [77,78]. Given the favorable bioactivity and joint retention characteristics demonstrated here, PEG-MnO_2 NPs may have potential to overcome the limitations of many current antioxidant therapies under investigation.

Most intra-articular therapies have focused on sustaining NP and/or drug levels within the joint for prolonged periods of time [22]. However, there is increasing appreciation for the need to improve localization of therapeutics to specific joint tissues [27,44]. In this work, ROS scavenging MnO_2 NPs were designed to localize to cartilage, which is highly vulnerable to oxidative stress. As mentioned previously, given the limited capacity of cartilage to repair, it is critical to provide chondroprotection to cartilage exposed to inflammation-induced oxidative stress. The development of cartilage targeted nanomaterials is still in the early stages of investigation [27]. Studies have demonstrated that substances with a small hydrodynamic size (< 15 nm in size) and positive surface charge, such as Avidin [79] or polyamidoamine (PAMAM) dendrimers [40], demonstrate full-depth penetration of cartilage explants, greater concentrations in articular cartilage than their neutral counterparts [41–43], and/or increase the joint retention of conjugated therapeutics after intra-articular injection [40]. Based on these findings, particles with similar charge and size properties but with ROS scavenging capabilities were fabricated. The synthesis method presented here was successful in generating MnO_2 NPs that were 10 – 15 nm in diameter and colloidally stable in biological media. We employed a similar synthesis method to those previously reported for generating 10 – 15 nm MnO_2 colloids for biomedical applications, however we used a PEGylation strategy for stabilizing the final NPs. Previous studies utilized albumin or hyaluronic acid to stabilize MnO_2 NPs, which led to a substantial increase in the particle size from 15 nm to 50 or 180 nm, respectively, as these macromolecules result in physical interactions and clustering of multiple MnO_2 NPs [36,48]. In contrast, the PEGylation of the MnO_2 NPs did not cause a substantial change in hydrodynamic size. In addition, the resulting particles retained a positive zeta potential to facilitate electrostatic interactions with the anionic cartilage tissue [40,44,45]. With the design criteria fulfilled, these particles demonstrated both penetration into cartilage ECM and colocalization with resident chondrocytes in both *in vitro* cartilage explants and *in vivo* after intra-articular injection. Furthermore, the NPs were retained in the joint for at least 7 days, whereas many small molecules are typically cleared within hours [22]. The longevity of the particles in the joint may also be related to their electrostatic interactions with the

anionic cartilage matrix [41,45]. The PEG-MnO_2 NPs have therefore demonstrated not only extended joint retention but also localization to the cartilage *in vivo*.

The application of inorganic nanomaterials within the joint is often accompanied by concerns of biocompatibility. As such, this study tested the cytocompatibility of MnO_2 NPs with numerous different assays and joint cells. In chondrocyte monolayers, cytocompatibility was demonstrated using both MTS and LDH even at concentrations 20 times the concentration used in the chondroprotection experiments. Furthermore, LIVE/DEAD and TUNEL staining both indicated minimal cytotoxicity of the NPs to cartilage biopsies *ex vivo*, and histological analysis showed no adverse effects to the cartilage *in vivo*. Cytocompatibility of the PEG-MnO_2 NPs was also confirmed with other “off-target” cell types that are present in the joint and possibly exposed to the NPs including synoviocytes, MSCs and macrophages (both cell line RAW 264.7 and primary BMDMs). In addition to preserving cell viability, the PEG-MnO_2 NPs did not trigger inflammatory cascades and actually downregulated TNF-α secretion by classically activated macrophages. This finding was consistent with *in vivo* studies, in that no synovitis was observed after intra-articular injection of the PEG-MnO_2 NPs. Given that studies have shown wear particles from orthopedic implants can stimulate macrophage infiltration and activation [80], in addition to studies that demonstrate that Mn-based substances can induce toxicity in human cells, such as neural [81,82], cell membrane [83,84] and other histopathological damage [85], this confirmation of biocompatibility across different studies was particularly important. Toxicity is typically dose dependent and further studies will be needed to determine the therapeutic window of the PEG-MnO_2 NPs. In addition to confirming cytocompatibility for intra-articular applications, the data presented here contributes to the growing body of work in which Mn-based nanomaterials are investigated for biomedical applications [33][36] [86].

The chondroprotective effects of the PEG-MnO_2 NPs were determined in an OA-mimicking cartilage explant model, which enabled the detection of structural degeneration of the ECM and concomitant NO production, as well as in cytokine-challenged chondrocyte monolayer, which enabled gene expression analysis. Together, these studies allowed us to start exploring possible mechanisms of action of these free-radical scavenging NPs within the overall oxidant-antioxidant systems of these cells. The findings from both these experiments corroborated with each other in several ways. For instance, treatment with PEG-MnO_2 NPs decreased iNOS gene expression in cytokine challenged chondrocytes and also decreased NO production in cytokine challenged cartilage explants. Moreover, the reduced expression of MMPs and ADAMTS genes by cytokine-challenged chondrocytes when treated with the PEG-MnO_2 NPs corroborates the biochemical data from the explant study whereby PEG-MnO_2 NPs significantly decreased release of GAGs in cytokine-challenged explants. The expression of anabolic genes, COL2 and ACAN, were maintained at baseline healthy levels in the presence of PEG-MnO_2 NPs, suggesting that the ECM protection observed in the cartilage explants can be attributed to the protection from oxidative stress rather than facilitation of any anabolic responses. It is noteworthy that the effects of the NPs were observed 2 days after the end of the initial treatment, even with continued exposure to IL-1β, suggesting that chondrocyte uptake of the NPs may be important. In addition to NP uptake, intracellular localization may play a role in the action of the PEG-MnO_2 NPs. Only 19% of NPs taken up by chondrocytes escaped endosomes after a 24-hour incubation period,

however, this was sufficient for affecting gene expression. Further characterization of the intracellular fate of the PEG-MnO_2 NPs is warranted to establish relationships between the cellular and subcellular particle location and chondroprotective mechanisms.

Gene expression analysis of antioxidants and upstream antioxidant regulators suggests the PEG-MnO_2 NPs may substitute or augment the chondrocytes' endogenous antioxidant capacity. Treatment with PEG-MnO_2 NPs generally downregulated antioxidant gene expression in the presence of IL-1β relative to control cytokine challenged chondrocytes. One exception to this trend was with CAT, which was surprising given that the role of CAT in decomposing H_2O_2 closely resembles that of the MnO_2 NPs. The expression of CAT was actually downregulated to similar extents in all groups relative to healthy control chondrocytes. A previous study that delved into the effects of IL-1β on antioxidant gene expression in bovine chondrocytes demonstrated the upregulation of GPX and MnSOD but downregulation of CAT within 24 hours of IL-1β incubation [55]. The upregulation of CAT protein activity was not observed until 96-hours due to the long half-life of the CAT [55]. Therefore, it is also possible that the experimental setup (72-hours exposure to IL-1β) used here was not sufficiently long to observe impacts on CAT activity. GPX, in addition to most upstream antioxidant regulators, were upregulated in response to IL-1β but maintained at healthy control levels upon treatment with PEG-MnO_2 NPs, suggesting the NPs serve an antioxidant role. The expression of two different isoenzymes of SOD were evaluated – MnSOD (SOD2), which serves to dismutase free radical superoxide anions generated by mitochondrial respiration [87], and ECSOD (SOD3), which catalyzes the dismutation of superoxide anions in the extracellular environment [88]. Upregulation of both isoenzymes in response to IL-1β was observed, though MnSOD upregulation occurred to a much greater extent (40-fold) than ECSOD (1.3-fold). Both isoenzymes were also downregulated by the treatment by PEG-MnO_2 NPs, suggesting an effect on both extracellular and intracellular ROS scavenging. These findings further underscore the need to understand the intracellular and extracellular distribution of the PEG-MnO_2 NPs and how it relates to ROS scavenging mechanisms and chondroprotective effects. The requirements for primarily intracellular or both intracellular and extracellular ROS scavenging will be important in further optimizing the particle design for therapeutic studies *in vivo*. An additional consideration is the duration by which the PEG-MnO2 NPs exert their antioxidant effects. It is possible that sustained downregulation of antioxidant capacities could upset the cells' homeostatic balance between ROS and antioxidants. This will be an important focus in future longer-term studies.

The uptake of NPs can often lead to transient ROS generation [89]. In our study the genes for antioxidant regulators HMOX1 and SREBP1 were upregulated in the presence of PEG-MnO_2 NPs without IL-1β. While this may indicate the particles alone could induce some changes suggestive of oxidative stress in the absence of inflammation, the totality of the cartilage viability, biochemistry, and histology results points to a particle system compatible with chondrocytes overall.

The *ex vivo* model in this study involved the usage of healthy bovine cartilage as controls which were then cytokine-challenged by a major pro-inflammatory cytokine mediator, IL-1β, present in OA pathogenesis to produce an OA mimic. This model was particularly useful in that it closely mimicked human cartilage thickness, therefore recapitulating the

uptake, transport kinetics, and retention that might be observed with human cartilage [44]. However, OA in reality is induced by a spectrum of cytokines and biomechanical cues - this complexity will be captured as the investigation transitions towards determining therapeutic impact of the NPs in *in vivo* OA models. Upon injection, particles will be exposed to the complex biochemical and mechanical interplay present in OA. It is encouraging to note that based on the *in vivo* biodistribution, the uptake by and accumulation in the articular cartilage was still observed. A greater accumulation of particles was found closer to the articular surface of the cartilage with fewer particles present at deeper zones. Given that oxidative stress and cartilage degradation are initiated in the articular surface and superficial zone (10 – 20% of depth) of articular cartilage [11,90,91], a higher concentration of the PEG-MnO_2 particles in this anatomical location may be advantageous. Going forward, timing of the administration of the NPs during the progression of the disease will be a critical consideration. Previous studies have demonstrated that ROS plays a pivotal role in the exacerbation of inflammatory events occurring after mechanically driven injuries to cartilage [11,92,93]. However, the characterization of intra-articular ROS over time and disease progression (using physical markers such as cartilage degeneration) has not yet been conducted in preclinical models. This information will be important for determining the optimal timing for the administration of the MnO_2 NPs.

In conclusion, this study presents a promising chondroprotective approach to mitigating oxidative stress in OA cartilage. PEG-MnO_2 NPs were engineered to enable cartilage penetration and chondrocyte uptake without inducing cytotoxicity or adverse effects *in vitro* and *in vivo*. The results indicate that the PEG-MnO_2 NPs have the potential to reduce inflammation-induced oxidative stress in cartilage with a resultant improvement in chondrocyte viability and ECM preservation. Given their joint retention time and ROS scavenging capacity, these NPs could be used to target oxidative stress mechanisms to treat or prevent OA, for example if administered soon after a joint injury that commonly precedes OA onset. Further investigation is required to ensure no long-term adverse effects to the redox balance of the cells, as well as optimization of targeting and biodistribution at the cellular and subcellular levels. There remains potential to combine the bioactive properties of the particles with other drugs to provide a dual-pronged delivery system. For instance, the intracellular localization of the NPs within chondrocytes could be further leveraged to deliver other chondroprotective agents that have intracellular targets, such as nucleic acids, to target multiple synergetic pathways in OA pathology.

Methods

NP Synthesis and Characterization.

MnO_2 NPs were synthesized by a 30-minute redox reaction of potassium permanganate (Acros Organics, Geel, Belgium) with poly(allylamine hydrochloride) (Alfa Aesar, Ward Hill, MA, USA) in a 1:1 concentration in water [47]. Conjugation of PEG to further stabilize the MnO_2 NPs was done by adding acrylate-polyethylene glycol succinimidyl valerate (PEG–SVA) (M.W 3400, Laysan Bio Inc., Arab, AL, USA) to the MnO_2 NPs at a 1:1 weight/weight ratio for 2-hours to form PEG-MnO_2 NPs. Fluorescently tagged particles were synthesized by conjugating the primary amines present on the PEG-MnO_2 NPs to

Alexa Fluor 488, 594, or 750 NHS Ester (Succinimidyl Ester) (Life Technologies, Carlsbad, CA, USA) in the presence of 1-ethyl-3-(3-dimethylaminopropyl)carbodiimide hydrochloride) (EDC) for 2-hours at room temperature.

Colloidal stability of PEG-MnO_2 NPs in phosphate buffered saline (PBS) and bovine synovial fluid (Animal Technologies, Tyler, TX, USA) was assessed grossly in ratios similar to that used in *in vitro* studies. The UV-visible absorption spectrum of 100 ug/mL potassium permanganate ($KMnO_4$) and MnO_2 NPs in water was measured on a spectrophotometer (Biotek Synergy HT, Winooski, Vermont, USA) between 200 and 800 nm. The absorption spectra of PEG-SVA, MnO_2 NPs, and PEG-MnO_2 NPs were also determined using Fourier-transform infrared spectroscopy (FTIR) (Perkin Elmer Frontier, Perkin Elmer, Waltham, MA, USA).

These NPs were characterized for size and zeta potential by Dynamic Light Scattering (DLS; Particle Sizing Systems, Port Richey, FL, USA). Measurements for DLS were conducted in water at 0.2 mg/mL for size and zeta potential at room temperature. Imaging of PEG-MnO_2 NPs by transmission electron microscopy (TEM) (Tecnai™ FEI Spirit TEM 120kV, ThermoFisher Scientific, Waltham, MA, USA) was conducted on negatively stained samples. Analysis of the size of the particles by TEM imaging was analyzed by ImageJ 1.51j8.

The thermal stability of the NPs and PEG and PAH polymers were determined by thermogravimetric analysis (TGA; Perkin Elmer Instruments model, STA 6000). The TGA thermograms were recorded for 10 – 15 mg of powder or lyophilized sample at a heating rate of 10 °C/min, in the temperature range of 10ºC to 600°C under nitrogen atmosphere.

PEG-MnO_2 NPs and Alexa Fluor 594 labeled PEG-MnO_2 NPs, in concentrations ranging from 0 to 10 μg/mL, were also characterized for scavenging capacity of 100 μM H_2O_2 after 1-hour in PBS by H_2O_2 colorimetric detection kits (Enzo Life Sciences, Farmingdale, NY, USA and Amplex Red Hydrogen Peroxide/Peroxidase Assay Kit (ThermoFisher, Waltham, MA, USA). Concurrent oxygen generation curves [94] from the scavenging of 100 μM H_2O_2 by PEG-MnO_2 NPs, in concentrations ranging from 0 to 10 μg/mL, over a 1-hour period were generated using sealed oxygen release chambers (Instech Laboratories, PA, USA).

Primary Bovine Cartilage Explants and Cells Extraction.

Primary bovine cartilage explants of 4 mm diameter were aseptically harvested from the femoral condyles and patellofemoral grooves of male bovine juveniles (Research87 Inc., Boylston, MA, USA), and washed in sterile PBS with 1% penicillin-streptomycin. The explants were maintained at 37°C and 5% carbon dioxide in chondro cyte media (Dulbecco's Modified Eagle Medium (DMEM) with 4.5 g/L glucose, 584 mg/L L-glutamine, 110 mg/L sodium pyruvate, 10 mM hydroxyethyl piperazineethanesulfonic acid (HEPES), 0.1 mM nonessential amino acids, 0.4 mM proline, 50 mg/L vitamin C, 10% fetal bovine serum (FBS), and 1% penicillin-streptomycin). Primary bovine chondrocytes were obtained by digestion of cartilage explants in 0.2% trypsin for 30 minutes and 0.2% collagenase II (Worthington Biochemical Corporation, Lakewood, New Jersey, USA)

digestion overnight. Enzymatic digestion was conducted at 37°C and 5% carbon dioxide on an orbital shaker at 40 RPM, and followed by cell straining, washing, and recovery.

Cell and Cartilage Explant Uptake of Fluorescently tagged PEG-MnO_2.

Primary bovine chondrocytes of Passage 1 were plated on glass cover slips at 31,250 cells/cm^2 seeding density with 0.1 mL chondrocyte media prior to uptake. Once cells reached confluency, Alexa Fluor 488 labeled PEG-MnO_2 NPs were added to the cells at 0, 5, 10, and 20 μg/mL in low serum chondrocyte media (1% FBS). Uptake of the NPs by bovine chondrocytes in 2D culture was evaluated by confocal fluorescent imaging (Zeiss LSM 710 Confocal Microscope, Jena, Germany) after 24-hours of incubation and multiple washes of the cells with sterile PBS. Nuclei were stained with Hoechst 33258, Pentahydrate (bis-Benzimide) (Life Technologies, Carlsbad, CA, USA) and lysosome stained with LysoTracker™ Red DND-99 (Life Technologies, Carlsbad, CA, USA). A Mander's split coefficient analysis for co-localization of NPs (green channel) with endolysosomes (red channel) was conducted using colocalization analysis on ImageJ 1.51j8 [95]. Uptake of the NPs by 3D bovine cartilage explants (through all sides) was also evaluated by adding Alexa Fluor 488 or 594 labeled PEG-MnO_2 NPs at 250 μg/mL in low serum chondrocyte media (1% FBS) to the explants for 24-hour followed by multiple washes with sterile PBS. Uptake of the NPs by explants was determined by counter-staining a tissue cross section taken through the center of each explant with Hoechst 33258, Pentahydrate (bis-Benzimide) (Life Technologies, Carlsbad, CA, USA) and imaging it by confocal fluorescent imaging (Zeiss LSM 710 Confocal Microscope, Jena, Germany).

Cell and Cartilage Explant Viability in Presence of PEG-MnO_2.

The cytotoxicity of PEG-MnO_2 NPs to various cell types was determined using a cell proliferation colorimetric assay, CellTiter 96® AQ^{ueous} One Solution Cell Proliferation Assay (MTS) (Promega, Madison, WI, USA). Cells at 80% confluency in 96-well plates were incubated in concentrations of PEG-MnO_2 NPs ranging from 0 to 100 μg/mL for 24-hours in cell specific media. Following this incubation, the cells were washed with PBS once before fresh media was added to the wells for incubation over 48-hours. The media was refreshed in each well 30 minutes prior to adding the MTS reagent. In each well, 0.02 mL of MTS reagent was added to 0.1 mL media, including control wells that did not contain any cells. Three hours after addition of the MTS reagent, the media with the MTS reagent from each well was transferred to a new plate and colorimetric analysis was conducted using a spectrophotometer (Biotek Synergy HT, Winooski, VT, USA) at 490nm wavelength.

The cytotoxicity of PEG-MnO_2 NPs to the following cell types that are present in the joint was determined (1) Primary bovine chondrocytes of Passage 1 were plated at 3,000 cells/well in a 96-well plate with 0.1 mL chondrocyte media. (2) The RAW 264.7 Abelson murine leukemia virus transformed macrophage cell line was purchased from American Type Culture Collection (Manassas, VA, USA) and cultured at 25,000 cells/well in a 96-well plate in 0.1 mL high glucose DMEM with 10 mM HEPES and 1% penicillin-streptomycin. RAW 264.7 cells were classically activated using 0.25 ng/mL lipopolysaccharide (Sigma Aldrich, St. Louis, MO, USA) and 0.5 ng/mL interferon gamma (Sigma Aldrich, St. Louis, MO, USA). (3) Rat BMDMs were harvested from the femurs of 3-month old Lewis rats (Charles

River Laboratories). To isolate and differentiate BMDMs, cells were treated with ACK lysis buffer (Invitrogen, Carlsbad, CA, USA), centrifuged, and resuspended in DMEM with 4.5 g/L glucose, 584 mg/L L-glutamine, 110 mg/L sodium pyruvatem 2mM L-glutamine, 10% fetal bovine serum (FBS), and 1% penicillin-streptomycin and 20 ng/mL rat macrophage colony stimulating factor (MCSF; Biolegend, San Diego, CA, USA). BMDMs were cultured at 37°C in a humidified incubator with 5% CO2 for 7 days before being dissociated using cell dissociation buffer (Invitrogen, Carlsbad, CA, USA) and seeded at 30,000 cells/well in a 96-well plate in 0.1 mL of fresh media. BMDMs were classically activated using 0.25 ng/mL lipopolysaccharide (Sigma Aldrich, St. Louis, MO, USA) and 0.5 ng/mL interferon gamma (Sigma Aldrich, St. Louis, MO, USA). (4) A human bone marrow-derived mesenchymal stem cell line was purchased from ScienCell (Carlsbad, CA, USA) and cultured at 3,000 cells/well in a 96-well plate in 0.1 mL DMEM with 1 g/L glucose, 584 mg/L L-glutamine, 110 mg/L sodium pyruvate, 10% hyclone FBS, 1% penicillin-streptomycin and 10 ng/μL human recombinant fibroblast growth factor (Peprotech, Rocky Hill, NJ, USA). (5) Primary bovine synoviocytes were obtained by 0.2% collagenase I (Worthington Biochemical Corporation, Lakewood, New Jersey, USA) digestion of bovine synovium overnight followed by cell straining and were cultured at 3,000 cells/well in a 96-well plate in 0.1 mL DMEM with 4.5 g/L glucose, 584 mg/L L-glutamine, 10% FBS, and 1% penicillin-streptomycin.

The cytotoxicity of PEG-MnO_2 NPs to all the above-mentioned cell types was also determined by quantification of lactate dehydrogenase (LDH) release using the CytoTox-ONE™ Homogeneous Membrane Integrity Assay (Promega, Madison, WI, USA). Cells at 80% confluency in 96-well plates were incubated in concentrations of PEG-MnO_2 NPs ranging from 0 to 100 μg/mL. Due to the high background conferred by serum in media and the 9-hour half-life of LDH, cell-specific media was not used for this measurement and instead cells were incubated in Opti-MEM Reduced Serum Media (ThermoFisher, Waltham, MA, USA) over a 6-hour period. This media was then removed from the cells and the CytoTox-ONE™ Reagent was added to the media. A stop solution was added before fluorescence was analyzed using a spectrophotometer (Biotek Synergy HT, Winooski, VT, USA) at an excitation wavelength of 560 nm and an emission wavelength of 590 nm.

The viability of cartilage explants following exposure to PEG-MnO_2 NPs (5 μg/mL) was determined using a LIVE/DEAD™ Viability/Cytotoxicity Kit for mammalian cells (ThermoFisher, Waltham, MA, USA). A thin section through the center of each explant was cut and incubated in 0.5 mL of saline containing 4 μM of red-fluorescent ethidium homodimer-1 and 2 μM of green fluorescent calcein-AM for 30 minutes. A z-stack of the fluorescence near the articular surface of each cartilage explant slice was evaluated by confocal fluorescent imaging (Zeiss LSM 710 Confocal Microscope, Jena, Germany). The percentage of live cells out of total number of cells was quantified using ImageJ 1.51j8.

To determine off-target effects, the changes in macrophage phenotype elicited by treatment of cells with PEG-MnO_2 NPs were determined. BMDMs were seeded at 30,000 cells/well in a 96-well plate in 0.1 mL of DMEM with 4.5 g/L glucose, 584 mg/L L-glutamine, 110 mg/L sodium pyruvate, 2mM L-glutamine, 10% fetal bovine serum (FBS), and 1% penicillin-streptomycin and 20 ng/mL rat macrophage colony stimulating factor (MCSF; BioLegend,

San Diego, CA, USA). After overnight adherence to the plate, the media was replaced with fresh media containing (1) no stimuli (2) 0.25 ng/mL lipopolysaccharide and 0.5 ng/mL interferon gamma for classical activation with concentrations of PEG-MnO_2 NPs between 0 and 100 μg/mL. After 24-hours incubation, the supernatants were collected and analyzed for rat TNF-α (BioLegend, San Diego, CA, USA).and IL-10 secretion (ThermoFisher Scientific, Waltham, MA, USA) by enzyme-linked immunosorbent assay (ELISA) following the manufacturer's instructions.

GAG and NO Measurement.

Fresh bovine cartilage explants were incubated in chondrocyte media over a 14-day period and challenged with 10 ng/mL human recombinant IL-1β (Peprotech, Rocky Hill, NJ, USA) in the presence and absence of 5 μg/mL PEG-MnO_2 NPs (Scheme 1). In the dosage study, explants were challenged with 10 ng/mL human recombinant IL-1β (Peprotech, Rocky Hill, NJ, USA) in the presence of 5, 10, 25, and 50 μg/mL PEG-MnO_2 NPs. The media was changed every 2 – 3 days. While the IL-1β was added with every media change for groups exposed to IL-1β, the PEG-MnO_2 was only added on day 0 and 7 for the relevant groups (Scheme 1). The media in which the explants were incubated was collected and stored at −80°C following every media change for the period of the experiment. These media samples were tested at the end for concentration of glycosaminoglycans (GAGs), a key component of cartilage extracellular matrix, and concentration of nitric oxide (NO), a key reactive nitrogen species (RNS) related to oxidative stress in OA. The concentration of GAGs in the expended media was quantified using Dimethylmethylene Blue Assay (Sigma Aldrich, St. Louis, MO, USA) and read using a spectrophotometer (Biotek Synergy HT, Winooski, Vermont, USA) at 525 nm wavelength. NO concentrations in the expended media were evaluated by using a Griess Reagent kit (ThermoFisher Scientific, Waltham, MA, USA) and colorimetrically assessed by spectrophotometer (Biotek Synergy HT, Winooski, VT, USA) at 528 nm. All absorbances were converted to concentrations using a standard curve and concentrations were normalized by final wet weights of the explants.

Histological Staining.

The bovine cartilage explants were fixed in 10% formalin in neutral buffered saline for 24 hours, washed and infused with paraffin, embedded in paraffin and sectioned by the Molecular Pathology Core at University of Florida (Gainesville, Florida, USA). Sections were stained for sulfated GAGs using a Safranin-O stain, counter-stained with Fast Green and sealed in Permount (ThermoFisher Scientific, Waltham, MA, USA). The presence of apoptotic cells within cartilage explants was assessed by Click-iT™ Plus TUNEL Assay for In Situ Apoptosis Detection with Alexa Fluor 488 dye (ThermoFisher Scientific, Waltham, MA, USA). A positive control for the TUNEL Assay incubating a bovine cartilage explant section with DNAse I. Both the extent of Safranin-O staining and number of apoptotic cells were quantified using ImageJ 1.51j8.

Quantitative RT-PCR.

Following the culture and treatment of bovine chondrocytes (Scheme 2), total RNA was extracted from the cells using RNEasy Mini Kit (Qiagen, Venlo, Netherlands) according to the manufacturer's instructions. RNA samples were reverse transcribed into cDNA

according to the manufacturer's instructions (iScript™ cDNA Synthesis Kit, Bio-Rad, Hercules, CA, USA). The samples were held at 25°C for 5 min, 46°C for 20 min and 95°C for 1 min.

Gene expression levels were quantified by Applied Biosystems™ QuantStudio™ 6 Flex Real-Time PCR System (Applied Biosystems, Life Technologies, Carlsbad, CA, USA). The assay was performed using the Fast SYBER® Green Master Mix (Applied Biosystems, Life Technologies, Carlsbad, CA, USA) according to the manufacturer's instructions. The sequences for the primers (Eurofins Genomics, Luxembourg City, Luxembourg) used are listed in Table 1. After an initial hold stage at 95°C for 20s, cDNA was amplified for 50 cycles at 95°C for 1s and 60°C for 20s, followed by the melt curve stage at 95°C for 15s, 60°C for 1 min, and 95°C for 15s. Relative expression levels of target genes were determined using the comparative C_T method. For each replicate, target gene expression was normalized to bovine 18S. Control bovine chondrocytes were used for baseline gene expression.

In Vivo Retention, Biocompatibility and Biodistribution in Healthy Animals.

For all *in vivo* studies, skeletally mature male Lewis rats (3 months, approximately 250 g) were obtained from Charles River Laboratories (Wilmington, MA, USA) and allowed to acclimate to the housing at the University of Florida for at least one week prior to any injections or surgeries. All procedures were performed in accordance with University of Florida Institutional Animal Care and Use Committee (IACUC).

For *in vivo* joint retention studies, 20 μL intra-articular injections of 5 mg/mL of Alexa Fluor 750 labeled PEG-MnO_2 NPs (suspended in saline) were conducted on both knees of 3 rats while 1 rat received 20 μL intra-articular injections of saline in both knees as a control for background fluorescence. Joint retention was monitored using an *In Vivo* Imaging System (IVIS, Perkin Elmer, Waltham, MA, USA) over 7 days. The average radiant efficiency of the particles in each left knee was estimated using a region of interest tool.

In a separate cohort, biodistribution within the knee and the organs was determined 11 days after 20 μL intra-articular injections of 5 mg/mL Alexa Fluor 750 labeled PEG-MnO_2 NPs (suspended in saline) in both knees of 3 rats and saline injection in both knees of 1 rat. The knee joints of each rat were dissected, and the following components of the knees were imaged to determine distribution of the NPs within the knee joint: the extensor mechanism (includes the fatpad, synovium, distal quadriceps and patellar ligament) and patella, femoral head, tibial plateau and meniscus. Furthermore, biodistribution of the NPs within the rat was determined by imaging the following organs: heart, lungs, spleen, liver and kidneys.

The distribution of the NPs in whole joint histology sections was also evaluated in another cohort of 2 rats. 20 μL intra-articular injections of 5 mg/mL of Alexa Fluor 594 labeled PEG-MnO_2 NPs was conducted on 3 knees while 1 knee received a 20 μL intra-articular injection of saline. The rats were euthanized 2 days post-injection and the whole joints from each rat were fixed for 2 days in 10% formalin in neutral buffered saline and decalcified in Cal-Ex (ThermoFisher Scientific, Waltham, MA, USA) for 4 days. The samples were infused with paraffin, embedded in paraffin and sectioned to 5 μm. The distribution of the

NPs in whole joint histological sections was visualized using confocal fluorescent imaging (Zeiss LSM 710 Confocal Microscope, Jena, Germany).

Long-term biocompatibility of the NPs in healthy rats was evaluated in another cohort of 3 rats. 20 μL intra-articular injections of 5 mg/mL of Alexa Fluor 750 labeled PEG-MnO_2 NPs were injected into the left knees of the 3 rats. After 6 weeks, the animals were euthanized and the whole joints were processed as mentioned previously to obtain whole joint sections. These sections were stained by Toluidine Blue and quantitative measures in the 2010 OARSI recommendations for the rat [63] was conducted by a blinded investigator using GEKO software, an open source tool developed by the Orthopaedic Biomedical Engineering Laboratory at University of Florida for evaluation of knee OA [64]. A saline injected knee from the whole joint distribution study was used as a control.

Statistics.

Statistical analysis was conducted in GraphPad PRISM 7.01 (La Jolla, CA, USA). Error bars indicate standard deviations. For the *in vitro* proliferation studies, a Dunnett's test was conducted while statistical comparison of means was conducted in GraphPad *via* one-way ANOVA with Tukey's multiple comparisons tests generally for all other studies (unless otherwise indicated in the figure caption). Statistical significance was determined as p-value < 0.05 with $\alpha = 0.05$.

Supplementary Material

Refer to Web version on PubMed Central for supplementary material.

Acknowledgements:

This material is based upon work supported by the 2016 University of Florida Clinical and Translational Science Institute (CTSI) Junior Faculty Award and National Institute of Arthritis and Musculoskeletal and Skin Diseases (NIAMS) R01AR071335. Additionally, the authors would like to acknowledge Ryan Jungels and Joseph Soto for their assistance on embedding and sectioning of histological samples, Khushboo Undavia for her assistance with various particle characterization procedures, Robert Accolla and the Diabetes Tissue Engineering Laboratory at University of Florida for their assistance with the collection of oxygen generation data and Sofia Goodrich and the Polymer Chemistry Characterization Laboratory at University of Florida for their assistance with collection of TGA data The raw/processed data required to reproduce these findings cannot be shared at this time as the data also forms part of an ongoing study.

References:

[1]. Lawrence RC, Felson D, Helmick C, Arnold L, Choi H, Deyo R, Gabriel S, Hirsch R, Hochberg M, Hunder G, Jordan J, Katz J, Kremers H, Wolfe F, Workgroup NAD, Estimates of the Prevalence of Arthritis and Other Rheumatic Conditions in the United States, Part II, Arthritis Rheum 58 (2008) 26–35. doi:10.1002/art.23176.Estimates. [PubMed: 18163497]

[2]. Hootman JM, Helmick CG, Projections of US prevalence of arthritis and associated activity limitations, Arthritis Rheum 54 (2006) 226–229. doi:10.1002/art.21562. [PubMed: 16385518]

[3]. Grover AK, Samson SE, Benefits of antioxidant supplements for knee osteoarthritis: Rationale and reality, Nutr. J 15 (2016). doi:10.1186/s12937-015-0115-z.

[4]. Collins JA, Diekman BO, Loeser RF, Targeting aging for disease modification in osteoarthritis, Curr. Opin. Rheumatol 30 (2018) 101–107. doi:10.1097/BOR.0000000000000456. [PubMed: 28957964]

[5]. Lepetsos P, Papavassiliou AG, ROS/oxidative stress signaling in osteoarthritis, Biochim. Biophys. Acta - Mol. Basis Dis 1862 (2016) 576–591. doi:10.1016/j.bbadis.2016.01.003.

[6]. Poulet B, Beier F, Targeting oxidative stress to reduce osteoarthritis, Arthritis Res. Ther 18 (2016) 15–16. doi:10.1186/s13075-015-0908-7. [PubMed: 26780830]

[7]. Bijlsma JWJ, Berenbaum F, Lafeber FPJG, Osteoarthritis: An update with relevance for clinical practice, Lancet 377 (2011) 2115–2126. doi:10.1016/S0140-6736(11)60243-2. [PubMed: 21684382]

[8]. Loeser RF, Aging processes and the development of osteoarthritis, Curr. Opin. Rheumatol 25 (2013) 108–113. doi:10.1097/BOR.0b013e32835a9428. [PubMed: 23080227]

[9]. Roach HI, The complex pathology of osteoarthritis: Even mitochondria are involved, Arthritis Rheum 58 (2008) 2217–2218. doi:10.1002/art.23635. [PubMed: 18668573]

[10]. Loeser RF, Collins JA, Diekman BO, Ageing and the pathogenesis of osteoarthritis, Nat. Rev. Rheumatol 12 (2016) 412–420. doi:10.1038/nrrheum.2016.65. [PubMed: 27192932]

[11]. Buckwalter JA, Anderson DD, Brown TD, Tochigi Y, Martin JA, The Roles of Mechanical Stresses in the Pathogenesis of Osteoarthritis: Implications for Treatment of Joint Injuries, Cartilage 4 (2013) 286–294. doi:10.1177/1947603513495889. [PubMed: 25067995]

[12]. Rosenbaum CC, O'Mathuna DP, Chavez M, Shields K, Antioxidants and anti-inflammatory Dietary Supplements for Osteoarthritis and Rheumatoid Arthritis, Altern. Ther 16 (2010) 32–40. http://www.aafp.org/afp/2008/0115/p177.html.

[13]. Canter PH, Wider B, Ernst E, The antioxidant vitamins A, C, E and selenium in the treatment of arthritis: A systematic review of randomized clinical trials, Rheumatology 46 (2007) 1223–1233. doi:10.1093/rheumatology/kem116. [PubMed: 17522095]

[14]. Dulbecco P, Savarino V, Therapeutic potential of curcumin in digestive diseases, 19 (2013) 9256–9270. doi:10.3748/wjg.v19.i48.9256.

[15]. Cheuk Y, Fu S, Mok S, Intra-articular injection of an antioxidant formulation did not improve structural degeneration in a rat model of post-traumatic osteoarthritis, J. Orthop. Transl 8 (2017) 25–31. doi:10.1016/j.jot.2016.08.001.

[16]. Elmali N, Esenkaya I, Harma A, Ertem K, Turkoz Y, Mizrak B, Effect of resveratrol in experimental osteoarthritis in rabbits, Inflamm. Res 54 (2005) 158–162. doi:10.1007/s00011-004-1341-6. [PubMed: 15883738]

[17]. Wang J, Chen JGJ, Effect of resveratrol on cartilage protection and apoptosis inhibition in experimental osteoarthritis of rabbit, Rheumatol. Int 32 (2012) 1541–1548. doi:10.1007/s00296-010-1720-y. [PubMed: 21327438]

[18]. Li W, Cai L, Zhang Y, Cui L, Shen G, Intra-Articular Resveratrol Injection Prevents Osteoarthritis Progression in a Mouse Model by Activating SIRT1 and Thereby Silencing HIF-2 a, J. Orthop. Res 1 (2015) 1061–1070. doi:10.1002/jor.22859.

[19]. Natarajan V, Madhan B, Tiku ML, Intra-Articular Injections of Polyphenols Protect Articular Cartilage from Inflammation-Induced Degradation: Suggesting a Potential Role in Cartilage Therapeutics., PLoS One 10 (2015) e0127165. doi:10.1371/journal.pone.0127165. [PubMed: 26046639]

[20]. Greenwald RA, Therapeutic benefits of oxygen radical scavenger treatments remain unproven, J. Free Radicals Biol. Med 1 (1985) 173–177. doi:10.1016/0748-5514(85)90115-1.

[21]. Greenwald RA, Oxygen radicals, inflammation, and arthritis: Pathophysiological considerations and implications for treatment, Semin. Arthritis Rheum 20 (1991) 219–240. doi:10.1016/0049-0172(91)90018-U. [PubMed: 2042055]

[22]. Evans CH, Kraus VB, Setton LA, Progress in intra-articular therapy, Nat. Rev. Rheumatol 10 (2014) 11–22. doi:10.1038/nrrheum.2013.159. [PubMed: 24189839]

[23]. Gammer W, Brobäck L-G, Clinical Comparison of Orgotein and Methylpredisolone acetate in the Treatment of Osteoarthrosis of the Knee Joint, Scand. J. Rheumatol 13 (1984) 108–112. doi:10.3109/03009748409100372. [PubMed: 6377491]

[24]. Kavanaugh TE, Werfel TA, Cho H, Hasty KA, Duvall CL, Particle-based technologies for osteoarthritis detection and therapy, (2016) 132–147. doi:10.1007/s13346-015-0234-2.

[25]. Kraus VB, Berenbaum F, Lieberman JR, Jones DG, Spitzer AI, Effects of a Single Intra-Articular Injection of a Microsphere Formulation of Triamcinolone Acetonide on Knee Osteoarthritis Pain, J. Bone Jt. Surg 100 (2018) 666–677.

[26]. Lauro MR, Crascí L, Sansone F, Cardile V, Panico AM, Puglisi G, Development and In Vitro Evaluation of an Innovative (Dietary Flavonoid Supplement) on Osteoarthritis Process, Oxid. Med. Cell. Longev (2017). doi:10.1155/2017/7503240.

[27]. Brown S, Kumar S, Sharma B, Intra-articular targeting of nanomaterials for the treatment of osteoarthritis, Acta Biomater (2019). doi:10.1016/j.actbio.2019.03.010.

[28]. Henrotin Y, Kurz B, Aigner T, Oxygen and reactive oxygen species in cartilage degradation: Friends or foes?, Osteoarthr. Cartil 13 (2005) 643–654. doi:10.1016/j.joca.2005.04.002. [PubMed: 15936958]

[29]. Davies CM, Guilak F, Weinberg JB, Fermor B, Reactive nitrogen and oxygen species in interleukin-1-mediated DNA damage associated with osteoarthritis, Osteoarthr. Cartil 16 (2008) 624–630. doi:10.1016/j.joca.2007.09.012. [PubMed: 17945515]

[30]. Broughton DB, Wentworth RL, Laing ME, Mechanism of Decomposition of Hydrogen Peroxide Solutions with Manganese Dioxide. II, J. Am. Chem. Soc 69 (1947) 744–747. doi:10.1021/ja01196a004. [PubMed: 20292459]

[31]. Moulton PJ, Hiran TS, Goldring MB, Hancock JT, Detection of protein and mRNA of various components of the NADPH oxidase complex in an immortalized human chondrocyte line, Br J Rheumatol 36 (1997) 522–529. [PubMed: 9189052]

[32]. Hiran TS, Moulton PJ, Hancock JT, Detection of superoxide and NAPDH oxidase in porcine articular chondrocytes, Free Radic. Biol. Med 23 (1997) 736–743. doi:10.1016/S0891-5849(97)00054-3. [PubMed: 9296450]

[33]. Bizeau J, Tapeinos C, Marella C, Larrañaga A, Pandit A, Synthesis and characterization of hyaluronic acid coated manganese dioxide microparticles that act as ROS scavengers, Colloids Surfaces B Biointerfaces 159 (2017) 30–38. doi:10.1016/j.colsurfb.2017.07.081. [PubMed: 28779638]

[34]. Tootoonchi MH, Hashempour M, Blackwelder PL, Fraker CA, Manganese oxide particles as cytoprotective, oxygen generating agents, Acta Biomater 59 (2017) 327–337. doi:10.1016/j.actbio.2017.07.006. [PubMed: 28688986]

[35]. Zhang M, Xing L, Ke H, He YJ, Cui PF, Zhu Y, Jiang G, Bin Qiao J, Lu N, Chen H, Jiang HL, MnO2-Based Nanoplatform Serves as Drug Vehicle and MRI Contrast Agent for Cancer Theranostics, ACS Appl. Mater. Interfaces 9 (2017) 11337–11344. doi:10.1021/acsami.6b15247. [PubMed: 28291320]

[36]. Song M, Liu T, Shi C, Zhang X, Chen X, Bioconjugated manganese dioxide nanoparticles enhance chemotherapy response by priming tumor-Associated macrophages toward m1-like phenotype and attenuating tumor hypoxia, ACS Nano 10 (2016) 633–647. doi:10.1021/acsnano.5b06779. [PubMed: 26650065]

[37]. Rothenfluh D, Bermudez H, O'Neil CP, Hubbell J, Biofunctional polymer nanoparticles for intra-articular targeting and retention in cartilage., Nat. Mater 7 (2008) 248–254. doi:10.1038/nmat2116. [PubMed: 18246072]

[38]. Levick JR, Flow through interstitium and other fibrous matrices, Q. J. Exp. Physiol 72 (1987) 409–437. doi:10.1113/expphysiol.1987.sp003085. [PubMed: 3321140]

[39]. Torzilli PA, Arduino JM, Gregory JD, Bansal M, Effect of proteoglycan removal on solute mobility in articular cartilage., J. Biomech 30 (1997) 895–902. [PubMed: 9302612]

[40]. Geiger BC, Wang S, Padera RF, Grodzinsky AJ, Hammond PT, Cartilage-penetrating nanocarriers improve delivery and efficacy of growth factor treatment of osteoarthritis, Sci. Transl. Med 10 (2018) eaat8800. doi:10.1126/scitranslmed.aat8800. [PubMed: 30487252]

[41]. Bajpayee AG, Wong CR, Bawendi MG, Frank EH, Grodzinsky AJ, Avidin as a model for charge driven transport into cartilage and drug delivery for treating early stage post-traumatic osteoarthritis, Biomaterials 35 (2014) 538–549. doi:10.1016/j.biomaterials.2013.09.091. [PubMed: 24120044]

[42]. Bajpayee AG, Scheu M, Grodzinsky AJ, Porter RM, Electrostatic interactions enable rapid penetration, enhanced uptake and retention of intra-articular injected avidin in rat knee joints, J. Orthop. Res 32 (2014) 1044–1051. doi:10.1002/jor.22630. [PubMed: 24753019]

[43]. Bajpayee AG, Quadir MA, Hammond PT, Grodzinsky AJ, Charge based intra-cartilage delivery of single dose dexamethasone using Avidin nano-carriers suppresses cytokine-induced catabolism long term, Osteoarthr. Cartil 24 (2016) 71–81. doi:10.1016/j.joca.2015.07.010. [PubMed: 26211608]

[44]. Bajpayee AG, Grodzinsky AJ, Cartilage-targeting drug delivery: can electrostatic interactions help?, Nat. Rev. Rheumatol 13 (2017) 183–193. doi:10.1038/nrrheum.2016.210. [PubMed: 28202920]

[45]. Brown S, Pistiner J, Adjei I, Sharma B, Nanoparticle properties for delivery to cartilage: the implications of disease state, synovial fluid, and off-target uptake, Mol. Pharm 16 (2019) 469–479. doi:10.1021/acs.molpharmaceut.7b00484. [PubMed: 28669194]

[46]. Vedadghavami A, Wagner E, Mehta S, He T, Zhang C, Bajpayee A, Cartilage penetrating cationic peptide carriers for applications in drug delivery to avascular negatively charged tissues, Acta Biomater 93 (2019) 258–269. doi:10.4172/2157-7633.1000305.Improved. [PubMed: 30529083]

[47]. Luo Y, Preparation of MnO_2 nanoparticles by directly mixing potassium permanganate and polyelectrolyte aqueous solutions, Mater. Lett 61 (2007) 1893–1895. doi:10.1016/j.matlet.2006.07.165.

[48]. Prasad P, Gordijo CR, Abbasi AZ, Maeda A, Ip A, Rauth AM, Dacosta RS, Wu XY, Multifunctional albumin-MnO2 nanoparticles modulate solid tumor microenvironment by attenuating hypoxia, acidosis, vascular endothelial growth factor and enhance radiation response, ACS Nano 8 (2014) 3202–3212. doi:10.1021/nn405773r. [PubMed: 24702320]

[49]. Stabellini G, De Mattei M, Calastrini C, Gagliano N, Moscheni C, Pasello M, Pellati A, Bellucci C, Gioia M, Effects of interleukin-1 b on chondroblast viability and extracellular matrix changes in bovine articular cartilage explants, 57 (2003) 314–319. doi:10.1016/S0753-3322(03)00038-6.

[50]. Daheshia M, Yao JQ, The interleukin 1β pathway in the pathogenesis of osteoarthritis, J. Rheumatol 35 (2008) 2306–2312. doi:10.3899/jrheum.080346. [PubMed: 18925684]

[51]. Abramson SB, Osteoarthritis and nitric oxide, Osteoarthr. Cartil 16 (2008) S15–S20. doi:10.1016/S1063-4584(08)60008-4. [PubMed: 18794013]

[52]. Rose BJ, Kooyman DL, A Tale of Two Joints : The Role of Matrix Metalloproteases in Cartilage Biology, Dis. Markers (2016). doi:10.1155/2016/4895050.

[53]. Stanton H, Rogerson F, East C, Golub S, Lawlor K, Meeker C, Little C, Last K, Farmer P, Campbell I, Fourie A, Fosang A, ADAMTS5 is the major aggrecanase in mouse cartilage in vivo and in vitro, Nature 434 (2005) 648–652. [PubMed: 15800625]

[54]. Majumdar MK, Askew R, Schelling S, Stedman N, Blanchet T, Hopkins B, Morris EA, Glasson SS, Double-Knockout of ADAMTS-4 and ADAMTS-5 in Mice Results in Physiologically Normal Animals and Prevents the Progression of Osteoarthritis, 56 (2007) 3670–3674. doi:10.1002/art.23027.

[55]. Mathy-Hartert M, Hogge L, Sanchez C, Deby-Dupont G, Crielaard J, Henrotin Y, Interleukin-1 b and interleukin-6 disturb the antioxidant enzyme system in bovine chondrocytes: a possible explanation for oxidative stress generation, Osteoarthr. Cartil 16 (2008) 756–763. doi:10.1016/j.joca.2007.10.009. [PubMed: 18291685]

[56]. Mazzetti I, Grigolo B, Pulsatelli L, Dolzani P, Silvestri T, Roseti L, Meliconi R, Facchini A, Differential roles of nitric oxide and oxygen radicals in chondrocytes affected by osteoarthritis and rheumatoid arthritis, Clin. Sci 101 (2001) 593–599. [PubMed: 11724645]

[57]. Regan E, Flannelly J, Bowler R, Tran K, Nicks M, Carbone BD, Glueck D, Heijnen H, Mason R, Crapo J, Extracellular superoxide dismutase and oxidant damage in osteoarthritis, Arthritis Rheum 52 (2005) 3479–3491. doi:10.1002/art.21387. [PubMed: 16255039]

[58]. Kansanen E, Kuosmanen SM, Leinonen H, Levonen A, Redox Biology The Keap1-Nrf2 pathway : Mechanisms of activation and dysregulation in cancer, Redox Biol 1 (2013) 45–49. doi:10.1016/j.redox.2012.10.001. [PubMed: 24024136]

[59]. Maicas N, Ferrandiz ML, Brines R, Cuadrado A, Koenders MI, Van Den Berg WB, Alcaraz MJ, Deficiency of Nrf2 Accelerates the Effector Phase, Antioxidants Redox Signal 15 (2011) 889–901. doi:10.1089/ars.2010.3835.

[60]. Lu T, Zong M, Fan S, Lu Y, Yu S, Fan L, Thioredoxin 1 is associated with the proliferation and apoptosis of rheumatoid arthritis fibroblast-like synoviocytes, Clin. Rheumatol 37 (2018) 117–125. doi:10.1007/s10067-017-3832-1. [PubMed: 28914370]

[61]. Yang G, Tian S, Luo J, Zheng J, Sun H, Gao Y, PRDX1 overexpression contributes to the protection on chondrocytes from IL-1β-induced apoptosis, Int. J. Clin. Exp. Med 10 (2017) 6538–6547.

[62]. Lorenz H, Wenz W, Ivancic M, Steck E, Richter W, Early and stable upregulation of collagen type II, collagen type I and YKL40 expression levels in cartilage during early experimental osteoarthritis occurs independent of joint location and histological grading, Arthritis Res. Ther 7 (2005) 156–165. doi:10.1186/ar1471.

[63]. Gerwin N, Bendele AM, Glasson S, Carlson CS, The OARSI histopathology initiative - recommendations for histological assessments of osteoarthritis in the rat, Osteoarthr. Cartil 18 (2010) S24–S34. doi:10.1016/j.joca.2010.05.030.

[64]. Kloefkorn HE, Jacobs BY, Xie DF, Allen KD, A graphic user interface for the evaluation of knee osteoarthritis (GEKO): an open-source tool for histological grading, Osteoarthr. Cartil 27 (2018) 114–117. doi:10.1016/j.joca.2018.09.005. [PubMed: 30287396]

[65]. Kavanaugh TE, Dailing EA, Cho H, Hasty KA, Duvall CL, Development of Optimized Copolymers and Delivery Formulations to Scavenge Reactive Oxygen Species and Prevent Joint Damage from Post-Traumatic Osteoarthritis, Osteoarthr. Cartil 25 (2017) S265–S266. doi:10.1016/j.joca.2017.02.447.

[66]. Shi Y, Hu X, Cheng J, Zhang X, Zhao F, Shi W, Ren B, Yu H, Yang P, Li Z, Liu Q, Liu Z, Duan X, Fu X, Zhang J, Wang J, Ao Y, A small molecule promotes cartilage extracellular matrix generation and inhibits osteoarthritis development, Nat. Commun 10 (2019). doi:10.1038/s41467-019-09839-x.

[67]. Chung MF, Chia WT, Wan WL, Lin YJ, Sung HW, Controlled Release of an Anti-inflammatory Drug Using an Ultrasensitive ROS-Responsive Gas-Generating Carrier for Localized Inflammation Inhibition, J. Am. Chem. Soc 137 (2015) 12462–12465. doi:10.1021/jacs.5b08057. [PubMed: 26391111]

[68]. Poole K, Nelson C, Joshi R, Martin J, Gupta M, Haws S, Kavanaugh T, Skala M, Duvall C, ROS-Responsive Microspheres for On Demand Antioxidant Therapy in a Model of Diabetic Peripheral Arterial Disease, Biomaterials 41 (2015) 166–175. doi:10.1016/j.biomaterials.2014.11.016.ROS-Responsive. [PubMed: 25522975]

[69]. Gupta MK, Martin JR, Werfel TA, Shen T, Page JM, Duvall CL, Cell protective, ABC triblock polymer-based thermoresponsive hydrogels with ROS-triggered degradation and drug release, J. Am. Chem. Soc 136 (2014) 14896–14902. doi:10.1021/ja507626y. [PubMed: 25254509]

[70]. Gupta M, Meyer T, Nelson C, Duvall C, Poly(PS-b-DMA) Micelles for Reactive Oxygen Species Triggered Drug Release, J. Control. Release 162 (2012) 591–598. doi:10.1038/jid.2014.371. [PubMed: 22889714]

[71]. Pu HL, Chiang WL, Maiti B, Liao ZX, Ho YC, Shim MS, Chuang EY, Xia Y, Sung HW, Nanoparticles with dual responses to oxidative stress and reduced pH for drug release and anti-inflammatory applications, ACS Nano 8 (2014) 1213–1221. doi:10.1021/nn4058787. [PubMed: 24386907]

[72]. Leonaviciene L, Kirdaite G, Bradunaite R, Vaitkiene D, Vasiliauskas A, Zabulyte D, Ramanaviciene A, Ramanavicius A, Asmenavicius T, Mackiewicz Z, Effect of gold nanoparticles in the treatment of established collagen arthritis in rats, Med 48 (2012) 91–101.

[73]. Gomes A, Datta P, Sengupta J, Biswas A, Gomes A, Evaluation of Anti-Arthritic Property of Methotrexate Conjugated Gold Nanoparticle on Experimental Animal Models, J. Nanopharmaceutics Drug Deliv 1 (2013) 206–211. doi:10.1166/jnd.2013.1015.

[74]. Ponnurangam S, O'Connell GD, Chernyshova IV, Wood K, Hung CTH, Somasundaran P, Beneficial effects of cerium oxide nanoparticles in development of chondrocyte-seeded hydrogel constructs and cellular response to interleukin insults, Tissue Eng. - Part A 20 (2014) 2908–2919. doi:10.1089/ten.tea.2013.0592. [PubMed: 24762195]

[75]. Chen Q, Feng L, Liu J, Zhu W, Dong Z, Wu Y, Liu Z, Intelligent Albumin–MnO_2 Nanoparticles as pH-/H2O2-Responsive Dissociable Nanocarriers to Modulate Tumor Hypoxia for Effective Combination Therapy, Adv. Mater (2016) 7129–7136. doi:10.1002/adma.201601902. [PubMed: 27283434]

[76]. Hu DR, Chen LJ, Qu Y, Peng JR, Chu BY, Shi K, Hao Y, Zhong L, Wang MY, Qian ZY, Oxygen-generating hybrid polymeric nanoparticles with encapsulated doxorubicin and chlorin e6 for trimodal imaging-guided combined chemo-photodynamic therapy, Theranostics 8 (2018) 1558–1574. doi:10.7150/thno.22989. [PubMed: 29556341]

[77]. Zhu W, Dong Z, Fu T, Liu J, Chen Q, Li Y, Zhu R, Xu L, Liu Z, Modulation of Hypoxia in Solid Tumor Microenvironment with MnO_2 Nanoparticles to Enhance Photodynamic Therapy, Adv. Funct. Mater 26 (2016) 5490–5498. doi:10.1002/adfm.201600676.

[78]. Yang G, Xu L, Chao Y, Xu J, Sun X, Wu Y, Peng R, Liu Z, Hollow MnO2 as a tumor-microenvironment-responsive biodegradable nano-platform for combination therapy favoring antitumor immune responses, Nat. Commun 8 (2017). doi:10.1038/s41467-017-01050-0.

[79]. Bajpayee AG, Scheu M, Grodzinsky AJ, Porter RM, A rabbit model demonstrates the influence of cartilage thickness on intra-articular drug delivery and retention within cartilage, J. Orthop. Res 33 (2015) 660–667. doi:10.1002/jor.22841. [PubMed: 25627105]

[80]. Lin T, Pajarinen J, Nabeshima A, Córdova L, Loi F, Gibon E, Lu L, Nathan K, Jämsen E, Yao Z, Goodman S, Orthopaedic wear particle-induced bone loss and exogenous macrophage infiltration is mitigated by local infusion of NF-κB decoy oligodeoxynucleotide, J. Biomed. Mater. Res. Part A 105 (2017) 3169–3175. doi:10.1016/j.physbeh.2017.03.040.

[81]. Cersosimo MG, Koller WC, The diagnosis of manganese-induced parkinsonism, Neurotoxicology 27 (2006) 340–346. doi:10.1016/j.neuro.2005.10.006. [PubMed: 16325915]

[82]. Kwakye GF, Paoliello MMB, Mukhopadhyay S, Bowman AB, Aschner M, Manganese-induced parkinsonism and Parkinson's disease: Shared and distinguishable features, Int. J. Environ. Res. Public Health 12 (2015) 7519–7540. doi:10.3390/ijerph120707519. [PubMed: 26154659]

[83]. Alhadlaq HA, Akhtar MJ, Ahamed M, Different cytotoxic and apoptotic responses of MCF-7 and HT1080 cells to MnO_2 nanoparticles are based on similar mode of action, Toxicology 411 (2019) 71–80. doi:10.1016/j.tox.2018.10.023. [PubMed: 30395893]

[84]. Hussain SM, Hess KL, Gearhart JM, Geiss KT, Schlager JJ, In vitro toxicity of nanoparticles in BRL 3A rat liver cells, Toxicol. Vitr 19 (2005) 975–983. doi:10.1016/j.tiv.2005.06.034.

[85]. Williams M, Todd G, Roney N, Toxicological Profile for Manganese, in: Atlanta Agency Toxic Subst. Dis. Regist, 2012: pp. 11–38. https://ntp.niehs.nih.gov/.

[86]. Gilad AA, Walczak P, McMahon MT, Hyon BN, Jung HL, An K, Hyeon T, Van Zijl PCM, Bulte JWM, MR tracking of transplanted cells with "positive contrast" using manganese oxide nanoparticles, Magn. Reson. Med 60 (2008) 1–7. doi:10.1002/mrm.21622. [PubMed: 18581402]

[87]. Candas D, Li JJ, MnSOD in Oxidative Stress Response-Potential Regulation *via* Mitochondrial Protein Influx, Antioxid. Redox Signal 20 (2013) 1599–1617. doi:10.1089/ars.2013.5305. [PubMed: 23581847]

[88]. Regan E, Flannelly J, Bowler R, Tran K, Nicks M, Carbone BD, Glueck D, Heijnen H, Mason R, Crapo J, Extracellular superoxide dismutase and oxidant damage in osteoarthritis, Arthritis Rheum 52 (2005) 3479–3491. doi:10.1002/art.21387. [PubMed: 16255039]

[89]. Fu PP, Xia Q, Hwang HM, Ray PC, Yu H, Mechanisms of nanotoxicity: Generation of reactive oxygen species, J. Food Drug Anal 22 (2014) 64–75. doi:10.1016/j.jfda.2014.01.005. [PubMed: 24673904]

[90]. Martin JA, McCabe D, Walter M, Buckwalter JA, McKinley TO, N-acetylcysteine inhibits post-impact chondrocyte death in osteochondral explants, J. Bone Jt. Surg. - Ser. A 91 (2009) 1890–1897. doi:10.2106/JBJS.H.00545.

[91]. Goodwin MJ, McCabe D, Sauter E, Reese E, Walter M, Buckwalter JA, Rotenone Induced, Impact Death Chondrocyte, J Orthop Res 28 (2013) 1057–1063. doi:10.1002/jor.21091.Rotenone.

[92]. Green DM, Noble PC, Ahuero JS, Birdsall HH, Cellular events leading to chondrocyte death after cartilage impact injury, Arthritis Rheum 54 (2006) 1509–1517. doi:10.1002/art.21812. [PubMed: 16649187]

[93]. Loeser RF, Molecular Mechanisms of Cartilage Destruction: Mechanics, Inflammatory Mediators, and Aging Collide, Arthritis Rheum 54 (2006) 1357–1360. papers2://publication/uuid/C9FC7547–7105-4320-BEF1–96AF744B58F1. [PubMed: 16645963]

[94]. Avgoustiniatos ES, Dionne KE, Wilson DF, Yarmush ML, Colton CK, Measurements of the effective diffusion coefficient of oxygen in pancreatic islets, Ind. Eng. Chem. Res 46 (2007) 6157–6163. doi:10.1021/ie070662y.

[95]. Manders E, Verbeek F, Aten J, Measurement of co-localization of objects in dual-colour confocal images, J. Microsc 169 (1993) 375–382.

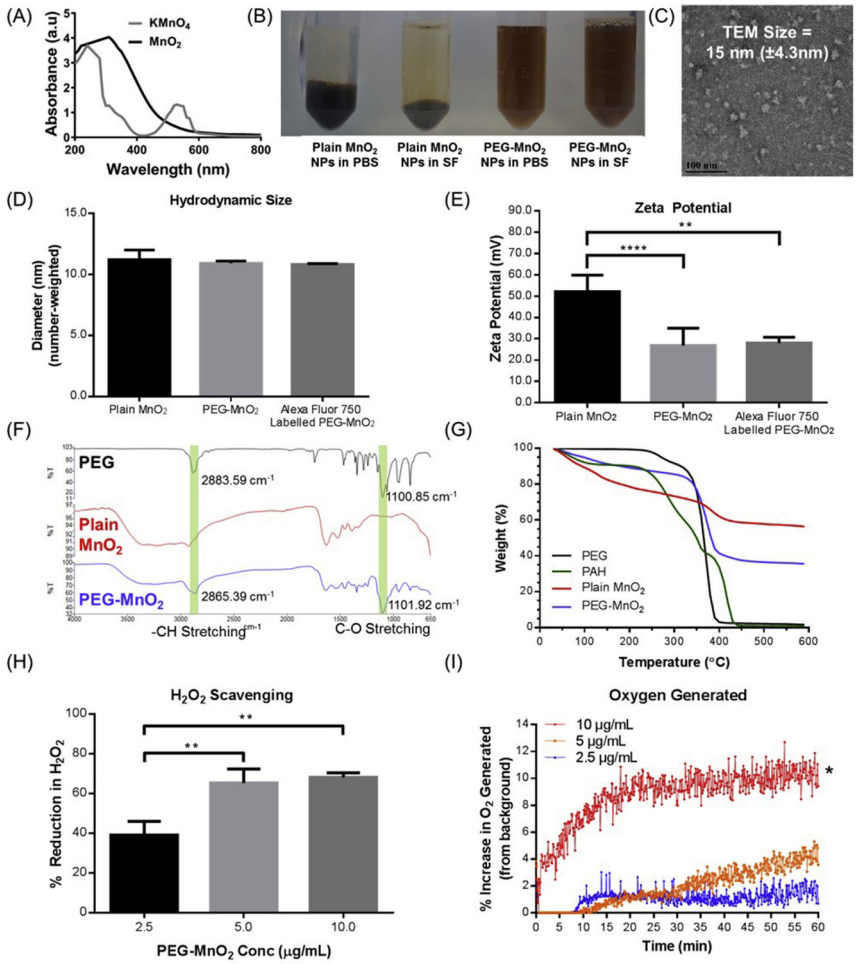

Fig. 1. Characterization of MnO2 NPs.

(A) The UV–visible absorption spectra of $KMnO_4$ and MnO_2 nanoparticles, measured on a spectrophotometer, indicated confirmation of reaction between KMnO4 and poly(allyl amine) to form MnO_2. (B) PEGylation of the MnO_2 NPs prevents them from aggregating in both phosphate buffered saline (PBS) and synovial fluid (SF) (C) The transmission electron microscopy (TEM) size of the PEG-MnO_2 NPs was 15.0 nm (±4.3 nm) (scale bar=100 nm) (D) In PBS, plain MnO_2 NPs, PEG-MnO_2 NPs and Alexa Fluor 750 labeled PEG-MnO_2 NPs had similar hydrodynamic diameter (number-weighted) (E) while the zeta potential of the NPs decreased when the plain MnO2 NPs were PEGylated (n = 4) when measured by dynamic light scattering (DLS), $^{**}p \leq 0.01$ and $^{****}p \leq 0.0001$. (F) PEGylation of the MnO_2NPs was confirmed by Fourier-transform infrared spectroscopy (FTIR) (G) Thermogravimetric analysis indicated that 35% of the PEG-MnO_2 NPs and 56% of plain MnO_2 NPs was composed of inorganic phase, MnO_2 (H) The different concentrations of PEG-MnO_2 NPs scavenged 100 μMH_2O_2 after an hour of incubation (n = 4), $^{**}p \leq 0.01$. (I) Synergistic oxygen generation studies indicated that more oxygen was generated as increasing concentrations of PEG-MnO_2 was added to 100 μMH_2O_2 (n = 2), $^{*}p \leq 0.05$ relative to the 2.5 μg/mL concentration.

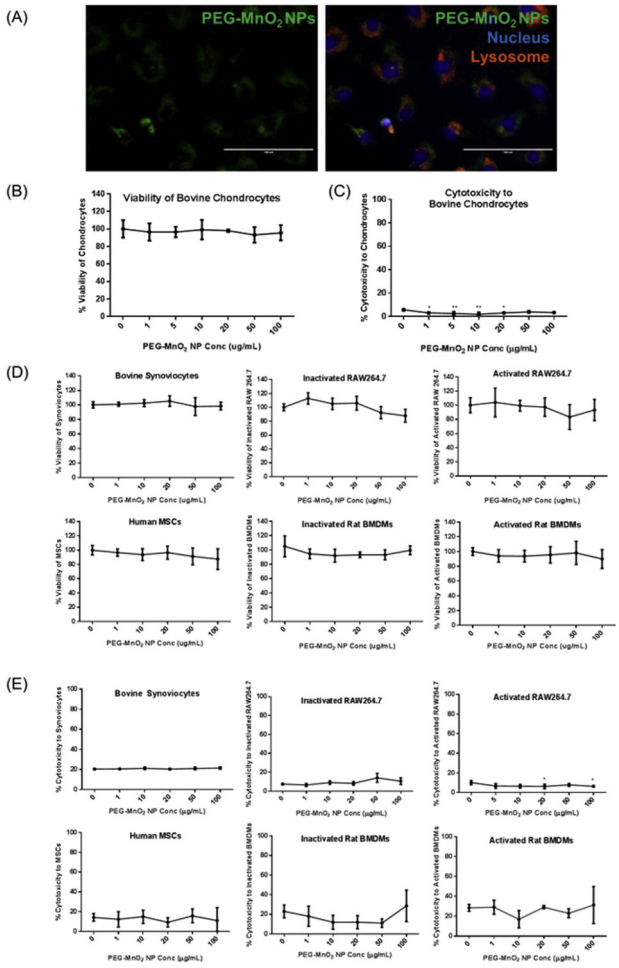

Fig. 2. Uptake and cytocompatibility of PEG-MnO_2 NPswith monolayers of joint cells.

(A) Primary bovine chondrocytes in monolayer showed uptake of Alexa Fluor 488 labeled PEG-MnO2 NPs (scale bar=100 μm). Nuclei were stained with Hoechst 33,258, Pentahydrate (bis-Benzimide) and lysosomes were stained with LysoTracker™ Red DND-99 (B) PEG-MnO_2 NPs were cytocompatible with primary bovine chondrocytes as assessed by MTS (n=6) (C) PEG-MnO_2 NPs were not cytotoxic to primary bovine chondrocytes as assessed by LDH (n=4) (D) PEG-MnO_2 NPs were cytocompatible with bovine synoviocytes, human MSCs, inactivated and classically activated macrophages (RAW264.7 cell line and primary rat bone marrow-derived macrophages (BMDMs)) as assessed by MTS (n=6) (E) PEG-MnO_2 NPs were not cytotoxic to bovine synoviocytes, human MSCs, inactivated and classically activated macrophages (RAW264.7 cell line and primary rat BMDMs) as assessed by LDH (n = 3–4). **p ≤ 0.01,***p ≤ 0.001 and ****p ≤ 0.0001 relative to the 0 μg/mL PEG-MnO_2 group for each cell type. (For interpretation of the references to color in this figure legend, the reader is referred to the Web version of this article.)

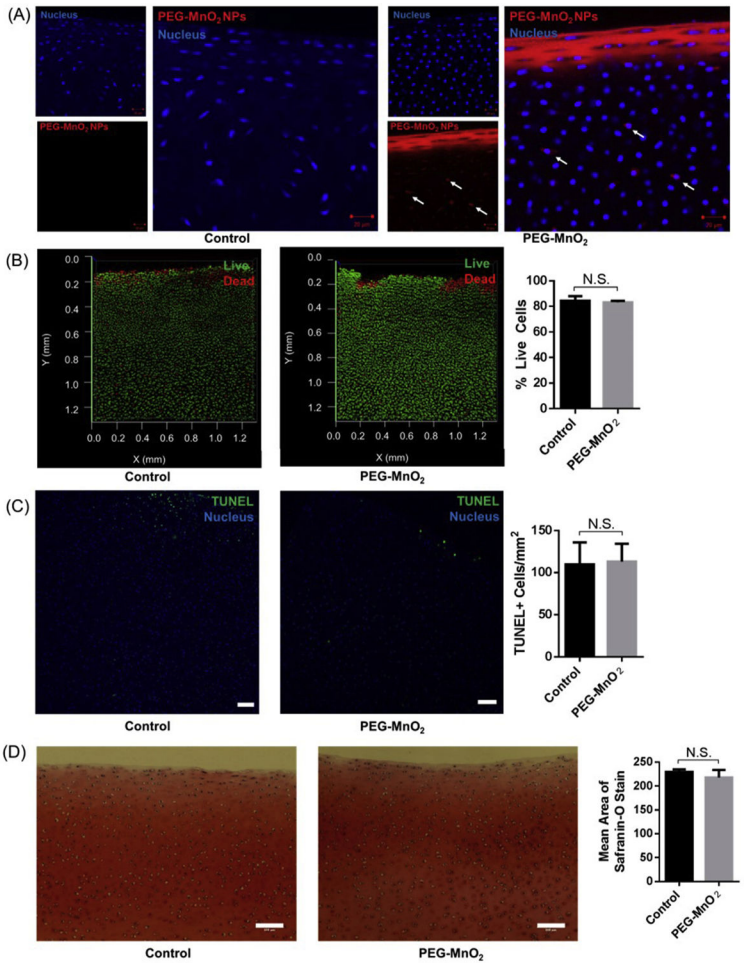

Fig. 3. Uptake and cytocompatibility of PEG-MnO_2 NPs with cartilage explants.

(A) Alexa 594 labeled PEG-MnO_2 NPs penetrated through cartilage biopsies, with endocytosis by resident chondrocytes (indicated by white arrows) following 24-h in culture (scale bar=20 μm) (B) Following 24-h of exposure to PEG-MnO_2 NPs, there was not a significant change in cell viability within experimental explants from control explants by LIVE/DEAD staining (n=3) or by (C) TUNEL Assay (n=3) (scale bar=100 μm). A positive control is shown in Fig. S4 (D) 24-h of exposure to PEG-MnO_2 NPs did not impact extracellular matrix as indicated by Safranin-0 staining (n=3) (scale bar=100 μm).

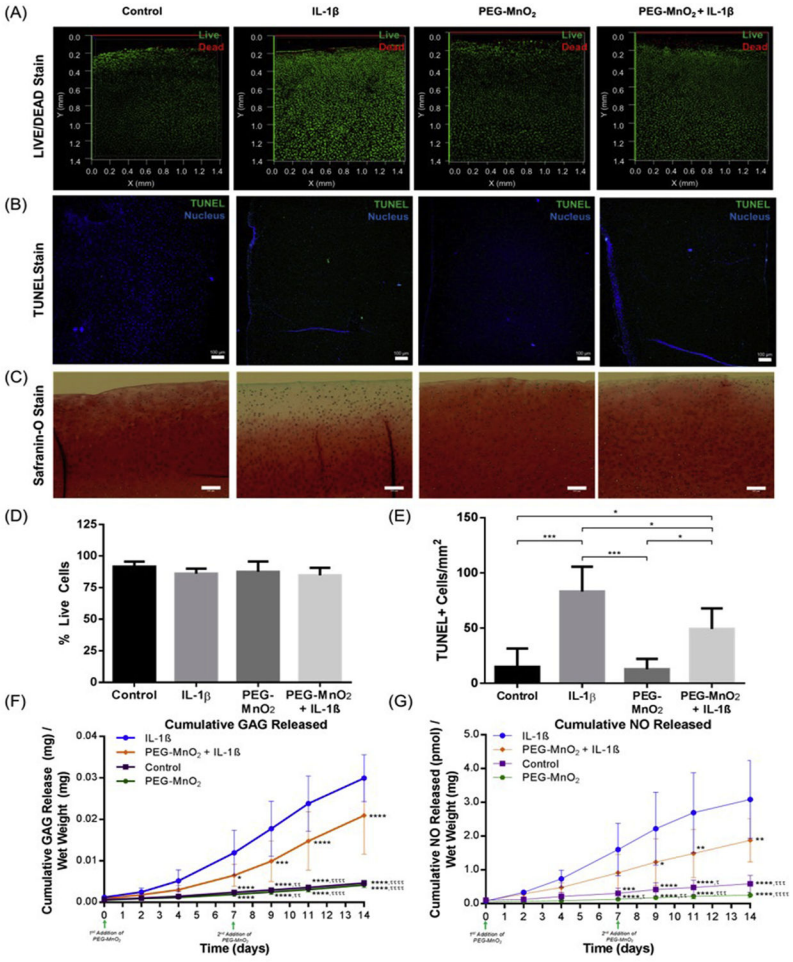

Fig. 4. Chondroprotective effects of PEG-MnO_2 NPs on cytokine challenged cartilage explants.

Following 2 weeks of exposure to different combinations of 10 ng/mL IL-1β and/or 5 μg/mL PEG-MnO_2 NPs, the bovine cartilage explants exhibited increased viability in the presence of PEG-MnO_2 NPs when challenged by IL-1β when measured by (A) LIVE/DEAD stain and by (B) TUNEL Assay (scale bar=100 μm). A positive control is shown in Fig. S4 (C) Increased staining of ECM components by Safranin-O in the cytokine challenged explants exposed to PEG-MnO_2 when compared to just the cytokine-challenged explants (scale bar=100 μm) was observed. (D) Quantification of viability by LIVE/DEAD staining (n=6) and (E) TUNEL Assay (n=6) reveal comparable viability but decreased apoptotic cells in the presence of PEG-MnO_2 NPs when cartilage is challenged by IL-1β, *p≤0.05 and ***p≤0.001 (F) 5 μg/mL PEG-MnO_2 NPs significantly decreased cumulative GAG loss by bovine cartilage explants challenged by 10 ng/mL 1L-1β (n=6). (G) 5 μg/mL PEG-MnO_2 also significantly decreased cumulative nitric oxide (NO) production by cytokine-challenged bovine cartilage explants (n = 6). A two-way ANOVA with Tukey's multiple comparisons test was used to determine statistical significance. *p ≤ 0.05,**p ≤ 0.01,***p ≤ 0.001,****p ≤ 0.0001 relative to IL-1β and ^{T}p≤0.05, ^{TT}p≤0.01, ^{TTT}p<0.001, ^{TTTT}p≤0.0001 relative to PEG-MnO_2 + IL-1β at each respective timepoint.

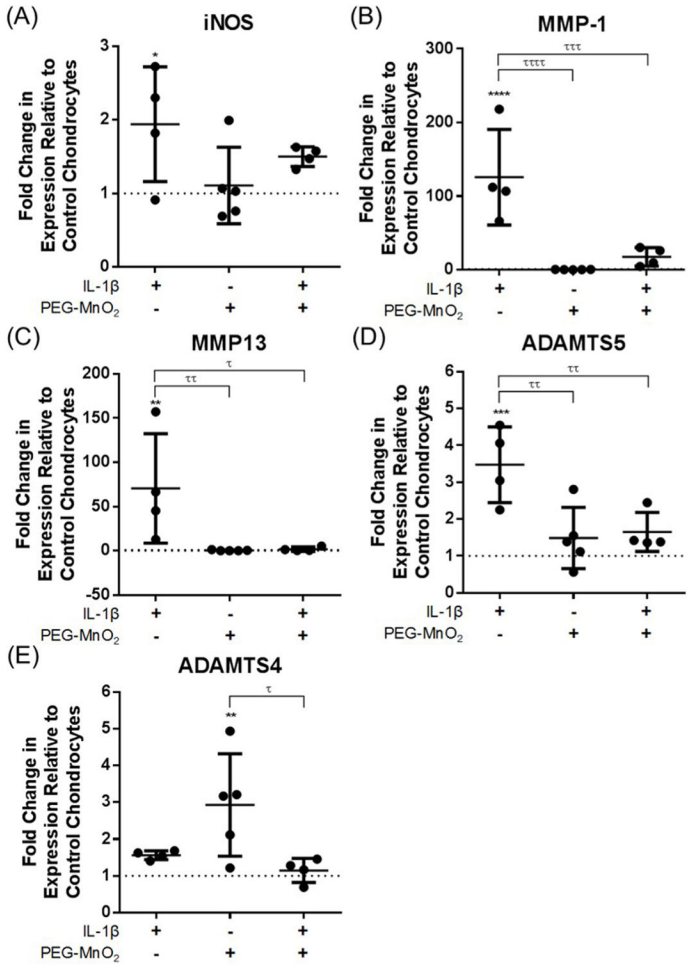

Fig. 5. Effects of PEG-MnO_2 NPs on expression of catabolic mediators in cytokine-challenged chondrocytes.

5 μg/mL PEG-MnO_2 NPs maintained the expression of catabolic mediators including (A) nitric oxide synthase (iNOS), (B) matrix metalloproteinases 3 (MMP3) and (C) 13 (MMP13) and (D) a disintegrin and metalloproteinase with thrombospondin motifs 5 (ADAMTS5) closer to baseline levels in bovine chondrocytes challenged by 10 ng/mL IL-1β. (E) The cytokine challenge did not upregulate expression of ADAMTS4. Each data point represents an experimental replicate with n = 4–5 for all genes.*$p \leq 0.05$,**$p \leq 0.01$,***$p \leq 0.001$,****$p < 0.0001$ relative to control chondrocytes and $^{T}p \leq 0.05$, $^{TT}p \leq 0.01$, $^{TTTT}p \leq 0.001$ and $^{TTTT}p \leq 0.0001$ between indicated groups.

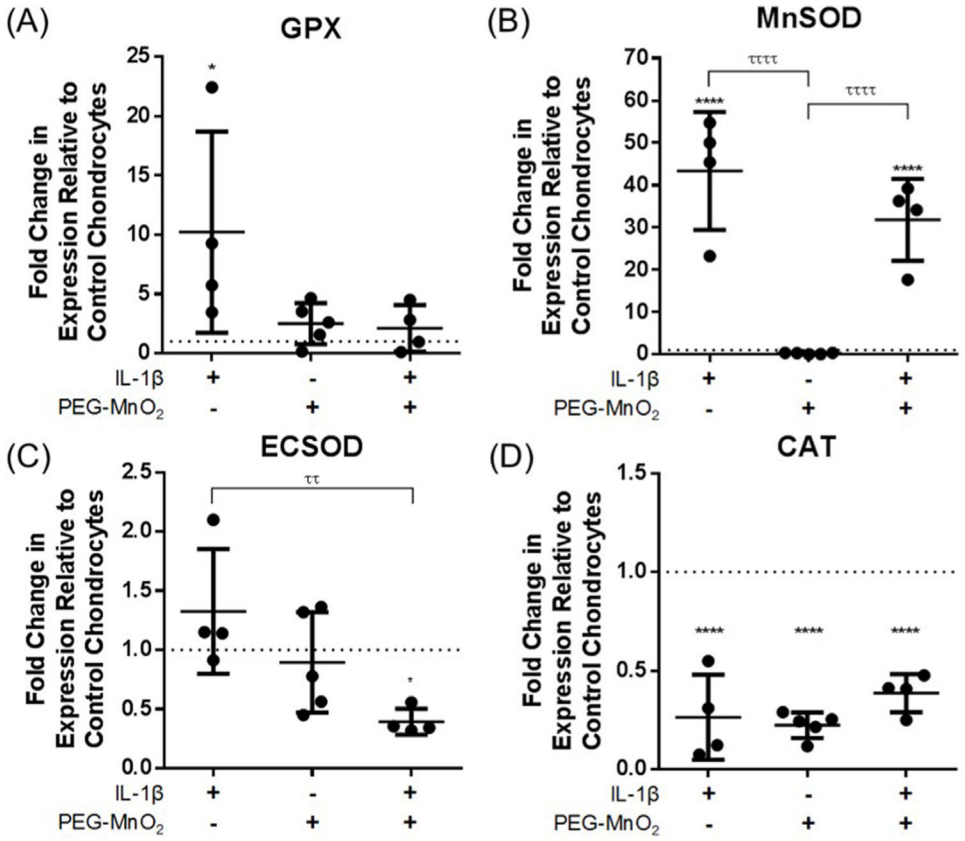

Fig. 6. Effects of PEG-MnO_2 NPs on antioxidant gene expression profiles of cytokine-challenged chondrocytes.

5 μg/mL PEG-MnO_2 NPs maintained the expression of antioxidants including (A) glutathione peroxidase (GPX). (B) Manganese superoxide dismutase (MnSOD) and (C) extracellular superoxide dismutase (ECSOD) closer to or below baseline levels in bovine chondrocytes challenged by 10 ng/mL IL-1β. (D) Catalase (CAT) is downregulated in all cases. Each data point represents an experimental replicate with n = 4–5 for all genes. *$p \leq 0.05$,**$p \leq 0.01$,***$p \leq 0.001$,****$p \leq 0.0001$ relative to control chondrocytes and $^{T}p \leq 0.05$, $^{TT}p \leq 0.01$, $^{TTT}p \leq 0.001$ and $^{TTTT}p \leq 0.0001$ between indicated groups.

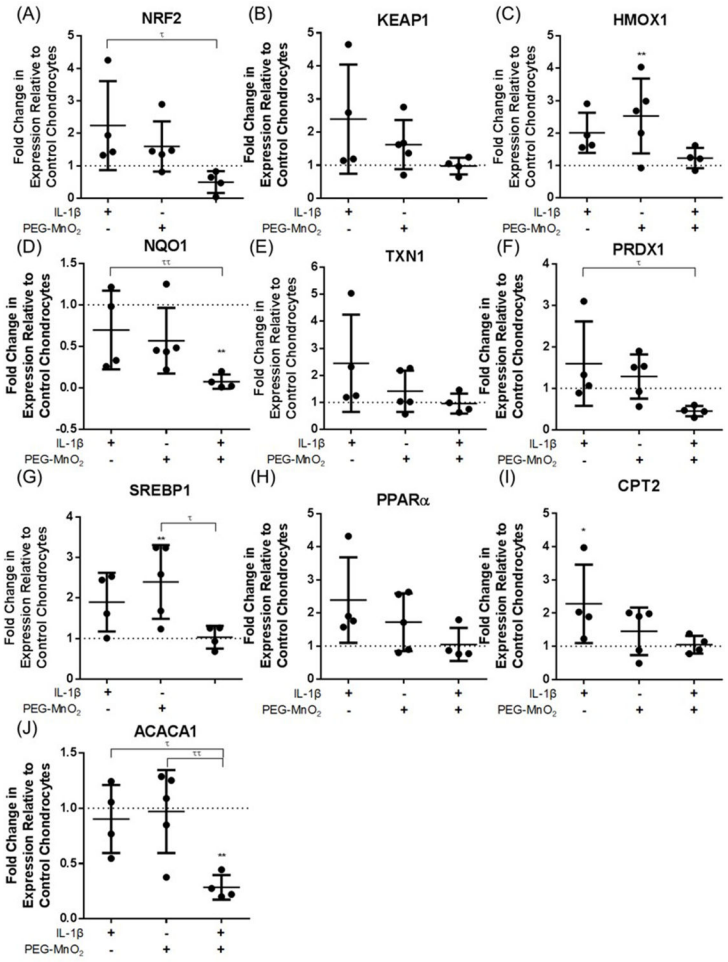

Fig. 7. Effects of PEG-MnO_2 NPs on expression of antioxidant mediators in cytokine-challenged chondrocytes.

5 μg/mL PEG-MnO_2 NPs maintained the expression antioxidant mediators including (A) Nuclear factor erythroid 2-like 2 (NRF2), (B) Kelch-like ECH-associated protein 1 (KEAP1), (C) Heme Oxygenase 1 (HMOX1), (D) NAD(P)H quinone dehydrogenase 1 (NQO1), (E) Thioredoxin 1 (TXN1), (F) Peroxiredoxin 1 (PRDX1) (G) Sterol regulatory element-binding protein 1 (SREBP1), (H) peroxisome proliferator-activated receptor a (PPARa), (I) carnitine palmitoyltransferase 2 (CPT2) and (J) acetyl-CoA carboxylase 1 (ACACA1) at or below baseline levels in bovine chondrocytes challenged by 10 ng/mL IL-1β. Each data point represents an experimental replicate with n = 4–5 for all genes. *$p \leq 0.05$,**$p \leq 0.01$ relative to control chondrocytes and $^{T}p \leq 0.05$, $^{TT}p \leq 0.01$ between indicated groups.

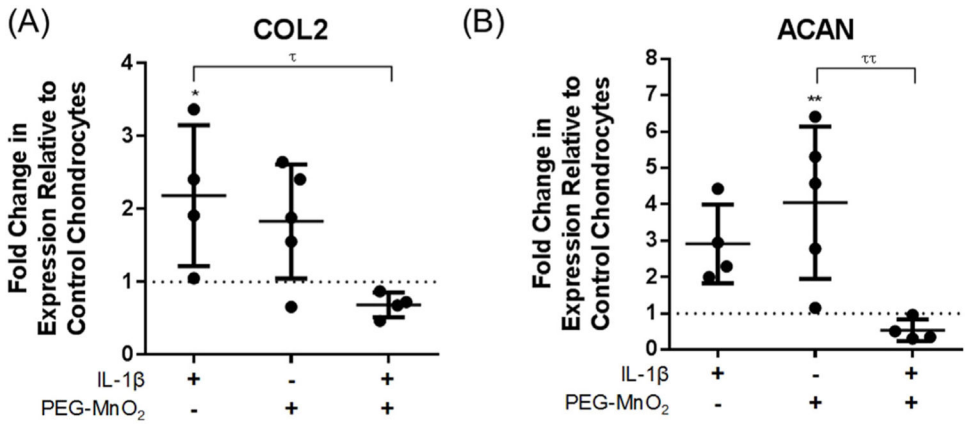

Fig. 8. Effects of PEG-MnO_2 NPs on anabolic gene expression by cytokine-challenged chondrocytes.

5 μg/mL PEG-MnO_2 NPs restored the expression of matrix building components including (A) collagen 2 (COL2) and (B) aggrecan (ACAN) closer to baseline levels in bovine chondrocytes challenged by 10 ng/mL IL-1β. Each data point represents an experimental replicate with n = 4–5 for all genes. *$p \leq 0.05$,**$p \leq 0.01$ relative to control chondrocytes and $^{T}p \leq 0.05$, $^{TT}p \leq 0.01$ between indicated groups.

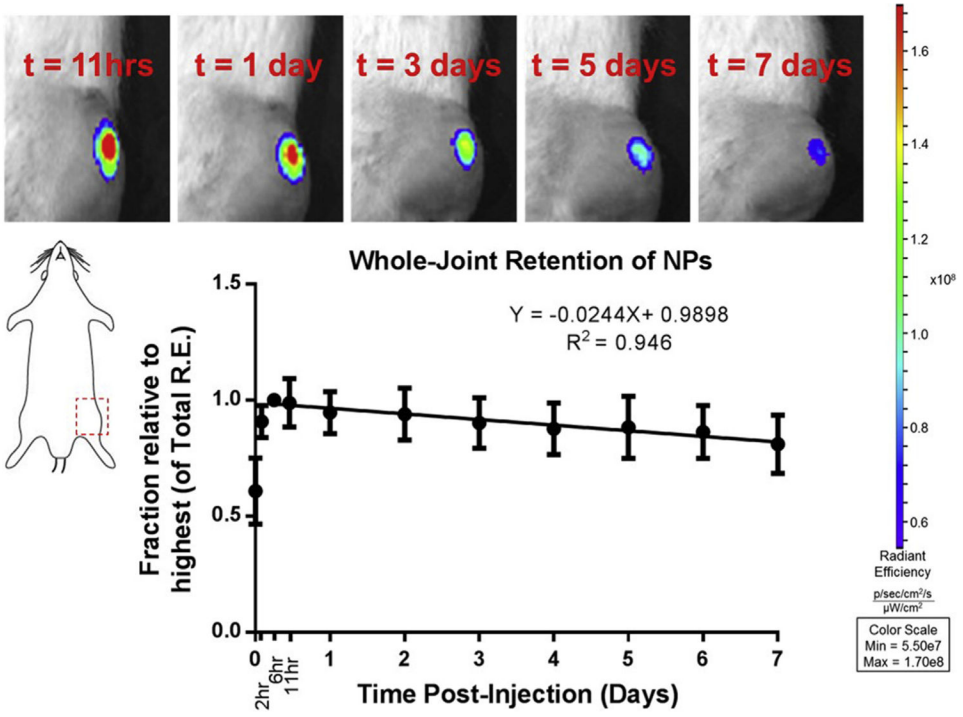

Fig. 9. Joint retention of PEG-MnO_2 NPs *in vivo*.

After *in vivo* injection in articular joints of Lewis Rats, Alexa Fluor 750 labeled PEG-MnO_2 NPs persisted in the joint for at least 7 days (n=6).

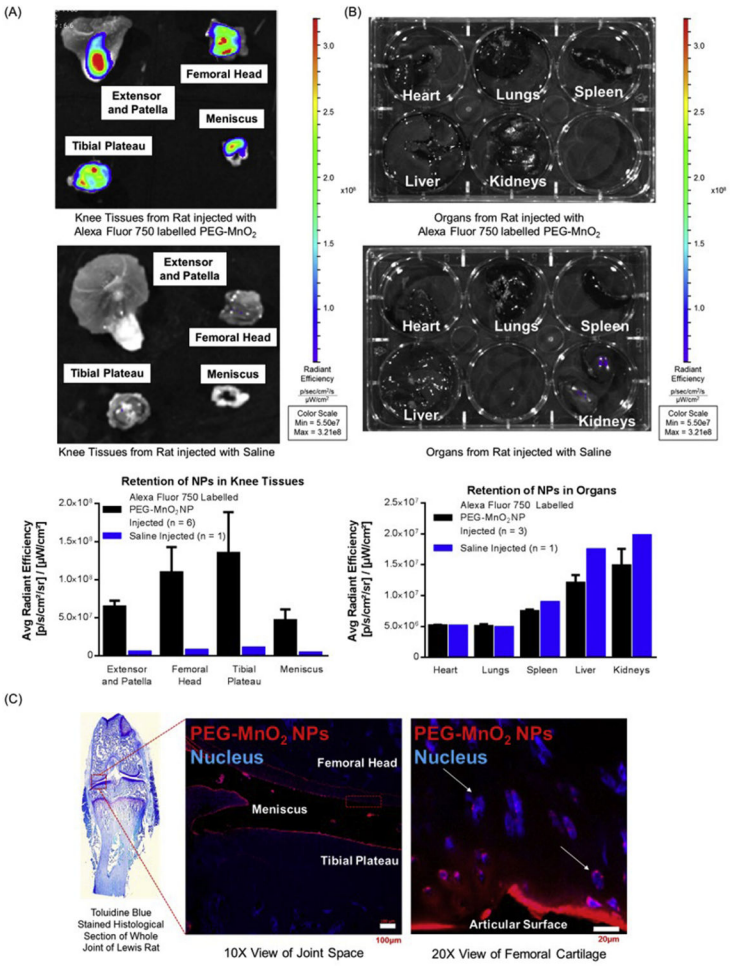

Fig. 10. Biodistribution of PEG-MnO_2 NPs *in vivo*

(A) Nanoparticle accumulation within the extensor mechanism and chondral surfaces (patella, femoral condyles, and tibial plateau) at the end of a 7-day study was observed (n=6 for injections of Alexa Fluor 750 labeled PEG-MnO_2 NPs and n=1 for saline injection) (B) NPs displayed minimal accumulation in key organs 7 days post-injection (n=3 for rats with injections of Alexa Fluor 750 labeled PEG-MnO_2 NPs and n=1 for rat with saline injection) (C) The Alexa Fluor 594 labeled PEG-MnO_2 NPs within knee joint 2 days post-injection in a histological sample was distributed in the chondral surfaces (scale bar=100 μm in 10X view and 20 μm in 20X view) with white arrows indicating uptake of NPs by resident chondrocytes in the femoral head.

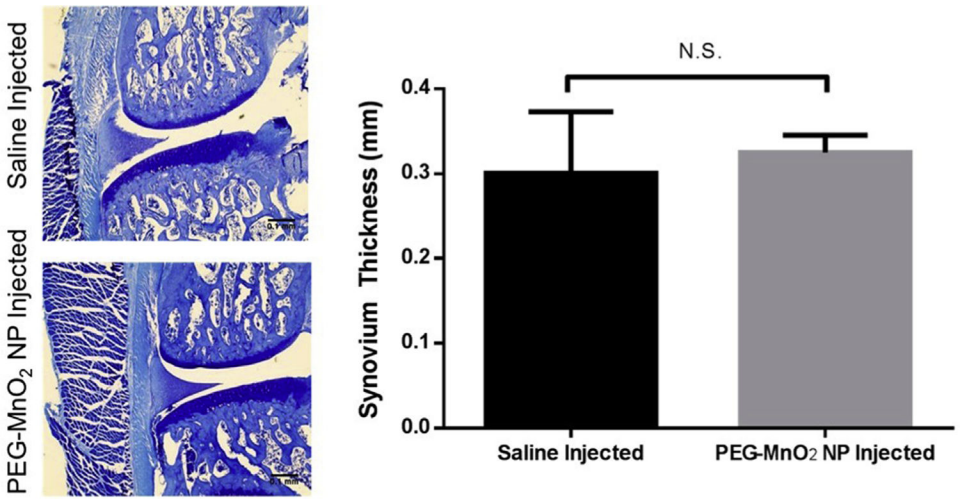

Fig. 11. Cytocompatibility of PEG-MnO_2 NPs *In Vivo*.

Representative histological images of toluidine stained knee sections (left, scale bar=0.1 mm) and representative parameter of evaluation of knee OA using GEKO software (right) show long-term cytocompatibility of the particles. No significant differences were found between the groups for cartilage matrix loss width 0%, 50% and 100% lesion depth, total cartilage degeneration width, significant cartilage degeneration width, zone 1, 2 and 3 depth ratio of lesion and osteophyte size.

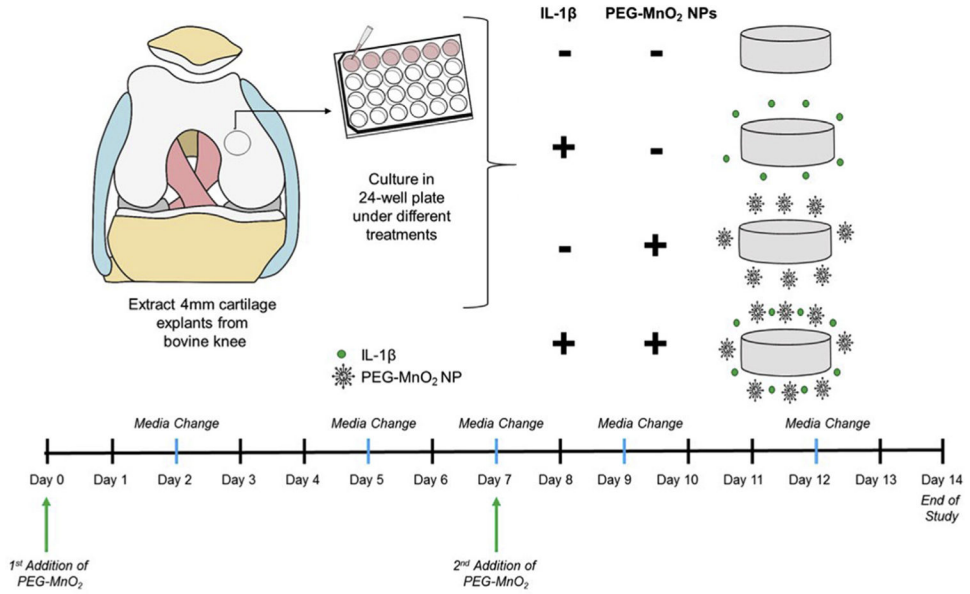

Scheme 1. Experimental plan for *in vitro* study of the therapeutic impact of PEG-MnO_2 on bovine cartilage explants.

Fresh 4mm diameter bovine cartilage explants were incubated in chondrocyte media over a 14-day period and challenged with 10 ng/mL human recombinant IL-1β in the presence and absence of 5 μg/mL PEG-MnO_2NPs. The media was changed every 2–3 days. While the IL-1p was added with every media change for groups exposed to IL-1β, the PEG-MnO_2 was only added on Day 0 and 7 for the relevant groups.

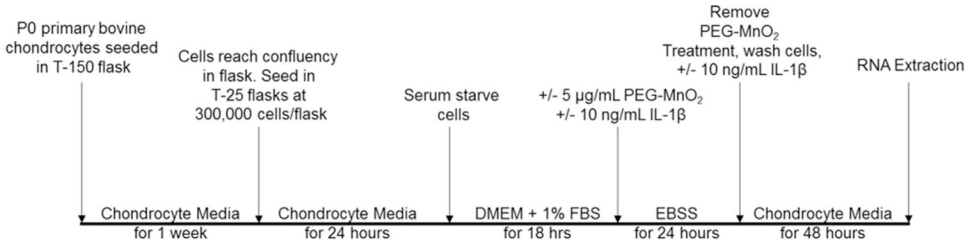

Scheme 2. Experimental plan for *in vitro* study of the impact of PEG-MnO_2 on gene expression of bovine chondrocytes.

Primary bovine chondrocytes were challenged with 10 ng/mL human recombinant IL-1β in the presence and absence of 5 μg/mL PEG-MnO_2 NPs. Primary bovine chondrocytes were serum starved for 24-h in low-serum chondrocyte media (1% FBS) before being challenged with 10 ng/mL human recombinant IL-1β in the presence and absence of a 1-time bolus 5 μg/mL PEG-MnO_2 NPs treatment in Earle's Balanced Salt Solution (EBSS) for 24-h. Treatments were removed and cells were washed before fresh chondrocyte media was added to them (cytokine-challenged cells continued to receive IL-1β but none of the groups continued to receive PEG-MnO_2 treatments). RNA was extracted after 48-h of incubation in the media.

Table 1

Primer sequences for genes tested with bovine chondrocytes.

Gene	Forward	Reverse
Catabolic Factors		
Bovine Inducible Nitric Oxide Synthase (iNOS)	5′-G GCAAGC ACCAC ATTGAG A-3′	5′-TGCGGCTGGATTTCGGA-3′
Bovine Matrix Metalloproteinase 1 (MMP1)	5′-G AC CAGC AATTTCC AAG ATTATAACTT-3′	5′-CC AAGGG AATG GCC AAA-3′
Bovine Matrix Metalloproteinase 13 (MMP13)	5′-C GCC AG AAGAATCTGTCTTTAAA-3′	5′-CC AAATTATGG AG GAGATGC-3′
Bovine A Disintegrin and Metalloproteinase with Thrombospondin Motifs 5 (ADAMTS-5)	5′-C AC CTCAG CCAC CATCACAG-3′	5′-AGTACTCTG GC CCG AAG GTC-3′
Bovine A Disintegrin and Metalloproteinase with Thrombospondin Motifs 4 (ADAMTS-4)	5 ′-CTC CATGACAACTC GAAGC A-3′	5′-CTAGGAGACAGTGCCCGAAG-3′
Anti-Oxidants		
Bovine Glutathione Peroxidase (GPX)	5′-G GACTACACC CAGATGAA-3′	5′-GTGGCGTCGTCACTTG-3′
Bovine Manganese Superoxide Dismutase (MnSOD)	5′-G CAAGTAAAC CGTC AGC-3′	5′-AACTACC AC CTCCTAGC-3′
Bovine Extracellular Superoxide Dismutase (ECSOD)	5′-G GCCTTCTTC CACCTTGA-3′	5′-GGAGCGGTACTTCCAGAC-3′
Bovine Catalase (CAT)	5′-GAACTGTCCCTACCGT-3′	5′-TCGTTGGCACTGTTGA-3′
ROS Modulators		
Bovine Nuclear Factor Erythroid 2-like 2 (NRF2)	5′-C AG CACAACAC ATAC CATCAG-3′	5′-TGC ATG CAGTC ATC GAAGTAC-3′
Bovine Kelch-like ECH-associated Protein 1 (KEAP1)	5-TCAC CAGG GAAGGATCTAC G-3′	5-AGC GGCTCAACAGGTAC AGT-3′
Bovine Heme Oxygenase 1 (HMOX1)	5′-C AAG GAGAACC CCGTCTACA-3′	5-CCAGACAG GTCTCC CAGGTA-3′
Bovine NAD(P)H Quinone Dehydrogenase 1 (NQO1)	5′-TCATCTCCAGAAAGGACATC-3′	5′-ACAGTCTCGGCAGGATACTG-3′
Bovine Thioredoxin 1 (TXN 1)	5′-AGCTGCC AAG ATG GTGAAAC-3′	5′-ACTCTGCAGCAACATCCTGA-3′
Bovine Peroxiredoxin 1 (PRDX1)	5-TGG ATC AACACACC CAAGAA-3′	5-GTCTCAGC GTCTCATCC ACA-3′
Bovine Sterol Regulatory Element-Binding Protein 1 (SREBP1)	5 ′-ACC GCTCTTC CATCAATGAC-3′	5-TTCAGC GATTTGCTTTTGTG-3′
Bovine Peroxisome Proliferator-Activated Receptor α (PPARAα)	5 ′-C CTACGG GAATGGCTTC ATA-3′	5′-GCACAATACCCTCCTGCATT-3′
Bovine Acetyl-CoA Carboxylase 1 (ACACA1)	5′-CTCTTC CG AC AGGTTCAAG C-3′	5′-ACC ATC CTGG CAAGTTTCAC-3′
Anabolic Factors		
Bovine Collagen 2 (COL2)	5′-G CATTGCCTAC CTGG AC GAA-3′	5-CGTTGGAG CCCTG GATGA-3′
Bovine Aggrecan (AGG)		
Housekeeping		
18S	5′-C GGCTAC CACATCC AAG GAA-3′	5′-GCTGGAATTACCG CG GCT-3′